
**A FIRST STEP TOWARD THE CALCULATION OF A
CONNECTIVITY MATRIX FOR THE GREAT BARRIER
REEF**

CHRIS BOWDEN

University of Reading
Department of Mathematics

Supervisor: Dr Emmanuel Hanert

August 2008

This dissertation is submitted to the Department of Mathematics in partial fulfilment of
the requirements for the degree of Master of Science

Abstract

Coral reef systems such as the Great Barrier Reef are fundamental to the food industry, tourism revenue and coastal protection of tropical regions. Due to recent human activity, the health of these coral reefs is under threat. It is therefore necessary to design marine reserves in order to protect and help sustain coral populations. An understanding of the connectivity between reefs or systems of reefs can help decide on the size and spacing of marine reserves.

To follow the paths of coral eggs released from reefs in simple domains, a particle tracking algorithm is developed in conjunction with a current hydrodynamic model of the Great Barrier Reef. The hydrodynamic model makes use of the $P_1^{NC} - P_1$ finite element formulation which is presented. Particle positions are updated by means of the Lagrangian algorithm.

This study suggests that the construction of connectivity matrices for reef systems should take into account both short and long range dispersal strategies by considering different species of coral and how their mechanisms of reproduction affect the dispersal time of their larvae.

Disclaimer

I confirm that this is my own work, and the use of all material from other sources has been properly and fully acknowledged.

Signed: _____ **Date:**_____

Acknowledgements

Firstly I would like to thank NERC for their generous grant, making it possible for me to study this course. I would also like to thank Emmanuel Hanert for all of his advice and ideas given while supervising this project.

I would like to thank all of my fellow MSc students for making the computer room an enjoyable and relaxing place to study. Many thanks also go to my girlfriend for all of the patience and reassurance she has given me throughout the course.

Lastly I would like to thank my Dad for all of the time, effort and money he spent on getting my program to run on all six computers in the house. Without his help I would not have managed to get all of the results needed before the time for the project ended.

Contents

Introduction	1
1 An unstructured-mesh hydrodynamic model of the GBR	6
1.1 The shallow water equations and boundary conditions	6
1.1.1 The shallow water equations	6
1.1.2 Boundary conditions	7
1.2 Criteria for the mesh	8
1.3 Numerical discretization of the SWEs	8
1.3.1 The $P_1^{NC} - P_1$ finite element formulation	9
1.3.2 The non-conforming mixed $P_1^{NC} - P_1$ finite element pair	12
1.3.3 Time integration scheme	14
2 Simulation of the transport of water-borne larvae	16
2.1 Choosing an advection-diffusion algorithm	17
2.1.1 Eulerian or Lagrangian?	17
2.2 Integration of the advection-diffusion algorithm with the model	18
2.2.1 The ‘point in a triangle’ test	18
2.2.2 Using the P_1 and P_1^{NC} weight functions to determine velocity at a point	21
2.2.3 Construction of the diffusion term	23
2.3 Testing the advection diffusion algorithm	24
2.4 Tracking coral eggs from islands	26

3	Results	32
3.1	Two island domain	32
3.1.1	Dispersal time = 4h (<i>Pocilloporids</i>)	33
3.1.2	Dispersal time = 24h - 72h (<i>Acroporids, Balanophyllia elegans</i>) . . .	35
3.2	Four island domain	36
3.2.1	Dispersal time = 4h (<i>Pocilloporids</i>)	36
3.2.2	Longer dispersal times	37
4	Discussion of results and conclusions	46
4.1	The two island domain	46
4.1.1	The four hour simulation	46
4.1.2	The 24-72 hour simulation	47
4.2	The four island domain	48
4.2.1	The four hour simulation	48
4.2.2	Longer simulations	48
4.3	Summary of conclusions	49
5	Further work	50
5.1	The modified Lagrangian algorithm	50
5.2	Areas representing the islands	51
5.3	A mortality rate	51
5.4	Different species of Coral	52
	Appendix A	52
	Bibliography	58

List of Figures

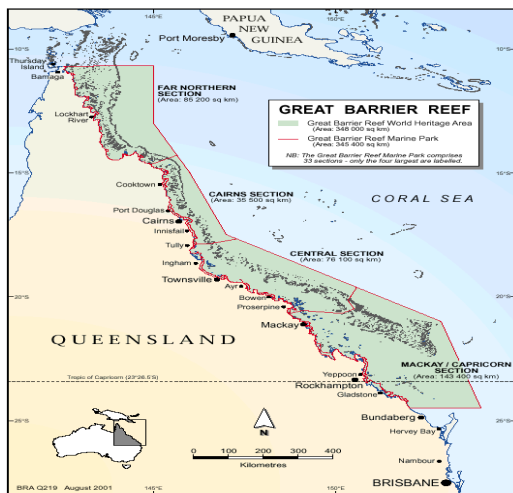
1	Map of locations of threatened corals reefs and sites that show signs of promise. Image taken from Bryant et al. (1998).	2
2	Map of locations of protected reef areas. Image taken from Bryant et al. (1998).	3
1.1	Model resolution	9
1.2	The linear conforming (left) and linear non-conforming (right) shape functions, image taken from [3]	12
1.3	Position of elevation and velocity nodes on an element	13
2.1	Each edge of a triangle splits 2-D space in half, image from [11]	19
2.2	How do we mathematically determine which point is in the triangle? Image from [11]	19
2.3	Shape functions	22
2.4	Stommel elevation fields at various time steps	25
2.5	Stommel velocity fields at various time steps	25
2.6	Energy in the Stommel simulation	25
2.7	A particle released into the Stommel simulation	26
2.8	Elevation and flow over the two island domain	27
2.9	Elevation and flow over the four island domain	28
2.10	A log/log plot of propagule duration vs. dispersal distance. Taken from [17].	29
2.11	Table of dispersal distances for different propagules, taken from [17].	30

2.12	Radii around islands inside which propagules are assumed to settle	31
3.1	Plot of the energy in the two island system against the time step	32
3.2	Minimum, maximum and mean distances dispersed from initial release points for the two island domain initial four hour period	34
3.3	Two islands, dispersal time ≈ 4 hours, diffusivity $k = 2.0\text{m}^2\text{s}^{-1}$	39
3.4	Two islands, dispersal time $\approx 4\text{h}$, diffusivity $k = 10.0\text{m}^2\text{s}^{-1}$	40
3.5	Energy in the four island system	41
3.6	Minimum, maximum and mean distances dispersed from initial release points for the two island 24-72 hour period	42
3.7	Two islands, dispersal time $\approx 24\text{-}72\text{h}$, diffusivity $k = 2.0\text{m}^2\text{s}^{-1}$	43
3.8	Two islands, dispersal time $\approx 24\text{h-}72\text{h}$, diffusivity $k = 50.0\text{m}^2\text{s}^{-1}$	44
3.9	Four islands, dispersal time $\approx 4\text{h}$, diffusivity $k = 10.0\text{m}^2\text{s}^{-1}$	45
5.1	Two islands, dispersal time $\approx 4\text{h}$, diffusivity $k = 25.0\text{m}^2\text{s}^{-1}$	54
5.2	Two islands, dispersal time $\approx 4\text{h}$, diffusivity $k = 50.0\text{m}^2\text{s}^{-1}$	55
5.3	Two islands, dispersal time $\approx 24\text{-}72\text{h}$, diffusivity $k = 10.0\text{m}^2\text{s}^{-1}$	56
5.4	Two islands, dispersal time $\approx 24\text{-}72\text{h}$, diffusivity $k = 25.0\text{m}^2\text{s}^{-1}$	57

Introduction

The Great Barrier Reef is located in the Coral Sea, off the coast of Queensland in North East Australia. It is composed of over 2500 individual reefs and 900 islands, stretching for over 2600km. The circulation over the Great Barrier Reef is mainly controlled by the complex topography of the continental shelf, the local wind and the shoreward South Equatorial current in the western Coral Sea. On meeting the Great Barrier Reef, the South Equatorial current splits at a bifurcation point into the northward flowing Coral Sea Coastal Current and the southward flowing East Australian Current (Wolanski, 1994).

Coral reefs occupy less than a quarter of a percent of the worlds marine environment, so



(a) Image from www.gbrmpa.gov.au



(b) Image from <http://www.anbg.gov.au>

what makes them so important? For a start, coral reefs are home to numerous different types of marine life, including over a quarter of all known fish species - within the Great Barrier Reef alone 1,500 species of fish and 4,000 species of mollusks have been counted (Bryant et al. 1998). But marine life is not the only thing dependent on the coral reefs.

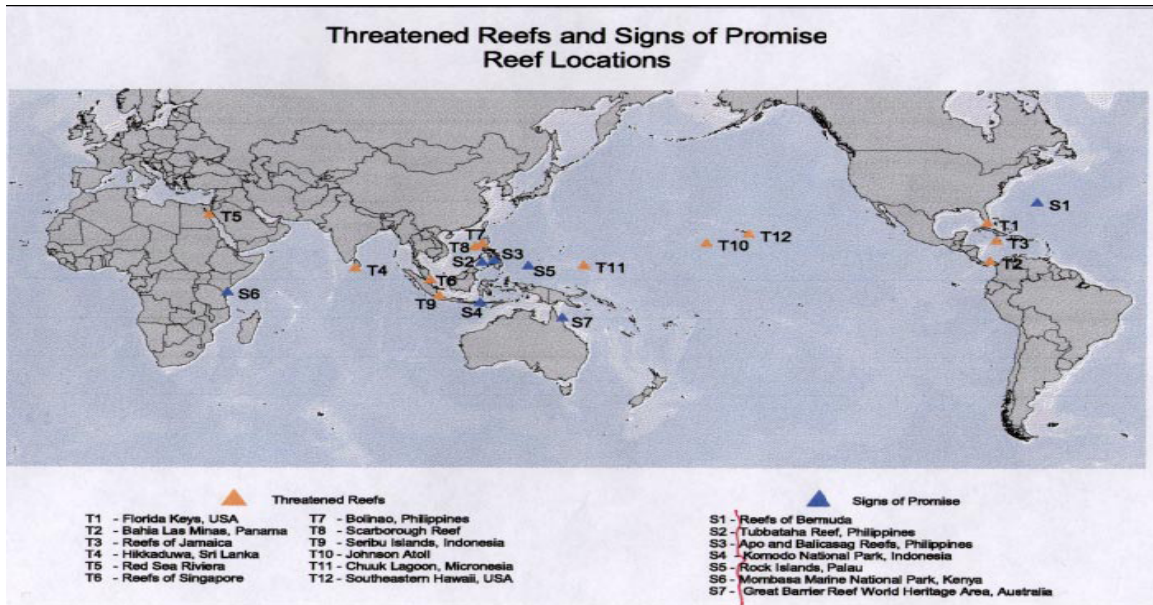


Figure 1: Map of locations of threatened corals reefs and sites that show signs of promise. Image taken from Bryant et al. (1998).

Fishing, tourism and economic resources of tropical areas are all built upon healthy coral ecosystems. Worldwide, the food, tourism revenue, coastal protection (barrier coral reefs protect shorelines from erosion and storm damage) and new medications that the reefs provide are worth over \$375 billion each year (Bryant et al., 1998), making them one of the most valuable ecosystems on Earth.

In 1998 an alarming report by Bryant et al. (1998) indicated that 58% of the worlds reefs were potentially threatened by human activity - ranging from coastal development and destructive fishing methods to overexploiting of resources, marine pollutions and runoff from inland deforestation and farming. Figure 1 gives a map of locations of reefs around the world and indicates those threatened and those that show signs of promise.

So what can be done to help sustain coral populations in these reefs? Part of the solution involves looking at the way corals reproduce and how different reefs rely on each other for sustainability. Once a year, certain types of corals, and many other benthic marine organisms, release propagules that spend time in the water column before settlement. During this period, ocean currents transport or disperse these propagules (Shanks, Grantham and

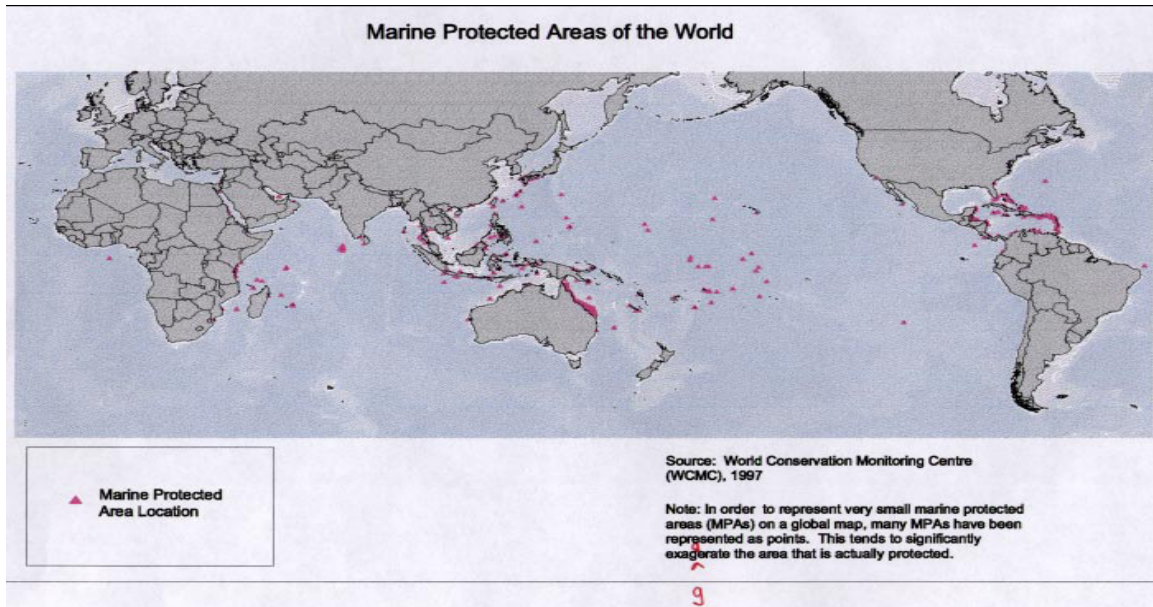


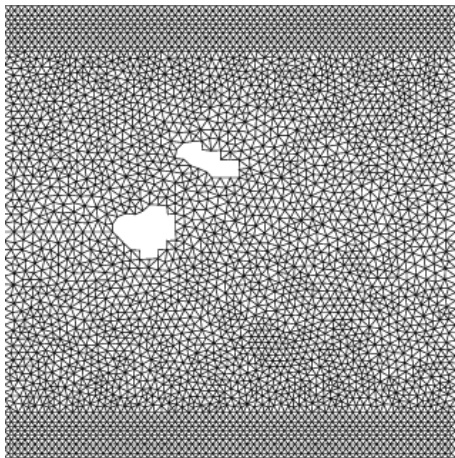
Figure 2: Map of locations of protected reef areas. Image taken from Bryant et al. (1998).

Carr 2003). The currents therefore control the transport of coral eggs between reefs, and hence determine the connectivity of reef populations. So what can be gained from investigating the connectivity between reef populations? Due to the damage inflicted to coral reefs by the various different processes described above, marine reserves must be designed to protect coral reef populations. Bryant et al., 1998, found that at least 40 countries did not have any marine protected areas for conserving their coral reef systems. A map of marine protected areas is given in Figure 2. The size and spacing of these reserves is not only critical to the sustainability of the protected populations but can also greatly influence unprotected populations outside of the reserves (Shanks et al., 2003). It is therefore important to have an understanding of how populations of corals in reefs or islands are being sustained. Is a reef or island self-replenishing or does it rely on the transport of coral eggs from other reefs and islands? To what extent does a reef or island replenish other populations? The answers to these questions can help determine how large marine reserves are made and how far apart they should be. Understanding the connectivity between coral reefs can help to identify which reefs or systems of reefs should be protected in order to enhance other unprotected populations.

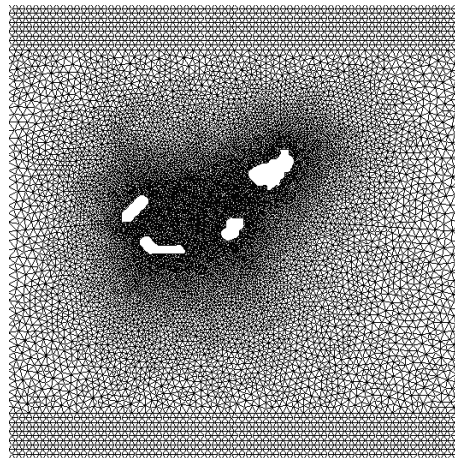
The purpose of this study is to develop a tool for use in conjunction with a current hy-

hydrodynamic model of the Great Barrier Reef that will track the paths of particles (or coral eggs) released from reefs. The model (provided by Emmanuel Hanert) simulates the flow over the Great Barrier Reef, and can also be used to simulate the flow throughout other simpler domains. Initially, a particle tracking algorithm will be built to run on a very simple test case - the Stommel model. This model creates a still, square lake which is then subjected to a surface wind forcing, producing a simple circulation. The model simulates the velocity and elevation fields, and the output is read using `gms` software (see www.geuz.org/gmsh for more information on this software).

Once the model has reached a steady state the particle tracking algorithm will be implemented. In this simple domain the behaviour of particles released into the domain is predictable, as their paths should be very similar the streamlines of the flow. Thus the algorithm is easily verified and at this point a more complex tracking algorithm and more exciting domains can be considered. The algorithm will be implemented and improved on two more square domains. Both domains comprise of two solid boundaries aligned with the y-axis and two open boundaries aligned with the x-axis. The first domain contains just two islands and the second contains four islands.



(a) Domain containing two islands, dimensions: $20\text{km} \times 20\text{km}$, min, max and mean element size: 0.23119, 0.505531 and 0.315272km



(b) Domain containing four islands, dimensions: $20\text{km} \times 20\text{km}$, min, max and mean element size: 0.0131661, 0.451218 and 0.162645km

In the domains pictured above, a flow is induced through the island by forcing the elevation on the two open boundaries. This flow is simulated by the ‘Connectivity’ test case

included in the model. The results of this study are in the form of connectivity matrices produced for each domain.

Chapter 1

An unstructured-mesh hydrodynamic model of the GBR

The model provided by Emmanuel Hanert is presented in [1] as a model that solves the discretized shallow water equations (SWEs) on a fully unstructured mesh of approximately 850,000 triangular elements. The model domain covered most of the GBR from the Great Keppel Island to the Forbes Island in the North^[1]. In this study, the model will run on the much smaller, simpler domains mentioned earlier that only contain a few islands. This chapter will outline the main features of the model and give examples of the output generated.

1.1 The shallow water equations and boundary conditions

1.1.1 The shallow water equations

The SWEs are comprised of the continuity equation and the horizontal momentum equations, they are presented below using the same notation as in [1]:

$$\begin{aligned} \frac{\partial \eta}{\partial t} + \frac{\partial(Hu)}{\partial x} + \frac{\partial(Hv)}{\partial y} &= 0, \\ \frac{\partial u}{\partial t} + u \frac{\partial u}{\partial x} + v \frac{\partial u}{\partial y} - fv + g \frac{\partial \eta}{\partial x} &= \frac{1}{H} \left(\frac{\partial}{\partial x} (\nu H \frac{\partial u}{\partial x}) + \frac{\partial}{\partial y} (\nu H \frac{\partial u}{\partial y}) \right) + \frac{\tau_x}{\rho H} - \frac{g \|\mathbf{u}\|}{C^2 H} u, \\ \frac{\partial v}{\partial t} + u \frac{\partial v}{\partial x} + v \frac{\partial v}{\partial y} + fu + g \frac{\partial \eta}{\partial y} &= \frac{1}{H} \left(\frac{\partial}{\partial x} (\nu H \frac{\partial v}{\partial x}) + \frac{\partial}{\partial y} (\nu H \frac{\partial v}{\partial y}) \right) + \frac{\tau_y}{\rho H} - \frac{g \|\mathbf{u}\|}{C^2 H} v, \end{aligned} \tag{1.1}$$

where the unknowns to be solved for are η , the sea surface elevation (positive upwards), u and v , the horizontal velocity components. The actual water depth is $H = h + \eta$, where h is the reference water depth below mean sea level. The Coriolis parameter, gravitational acceleration, horizontal eddy viscosity and mean water density are f , g , ν and ρ respectively. The wind stress at the surface of the sea is $\tau = (\tau_x, \tau_y)$. The bottom stress term is $\frac{g}{C^2 H} \|\mathbf{u}\| \mathbf{u}$, where $C = \frac{H^{\frac{1}{6}}}{n}$ is the Chezy coefficient which is determined by n the Manning roughness coefficient.

1.1.2 Boundary conditions

Alongside the above system of partial differential equations, initial and boundary conditions must be supplied so that the problem we are solving is well posed. Along the impermeable boundaries (islands and reefs), a zero mass flux and a tangential momentum flux proportional to the mean tangential velocity is imposed:

$$\begin{cases} u_n = 0, \\ \nu \frac{\partial u_s}{\partial n} + \alpha u_n = 0, \end{cases}$$

where s corresponds to the direction tangential to the boundary and n corresponds to the direction normal to the boundary - thus u_s and u_n are the horizontal components of velocity in these directions. Essentially, the first condition ensures that there is no flow through solid boundaries, while the second takes into account the fact that the boundaries are not smooth, so the flow along a boundary experiences a drag and is therefore slowed.

Conditions also need to be imposed on the open boundaries. For the GBR, measurements of the sea surface elevation at some locations in the Coral Sea can be used to force the tides and mean currents on the open boundaries^[1]. Where open boundaries are present in this study's simpler domains, a flow is induced into the domain by forcing the elevation on these boundaries. It is noted in [1] that the influence of initial conditions becomes negligible after some time, due to exchanges with the Coral Sea and frictional and viscous dissipations. This also holds true in the simpler test cases presented, with exchanges with the open boundaries rather than the Coral Sea specifically.

1.2 Criteria for the mesh

The model is based on an unstructured mesh, and so the size and shape of the triangular elements can be easily modified, allowing for variable resolution. The question is, where is fine resolution needed and where is coarse resolution needed?

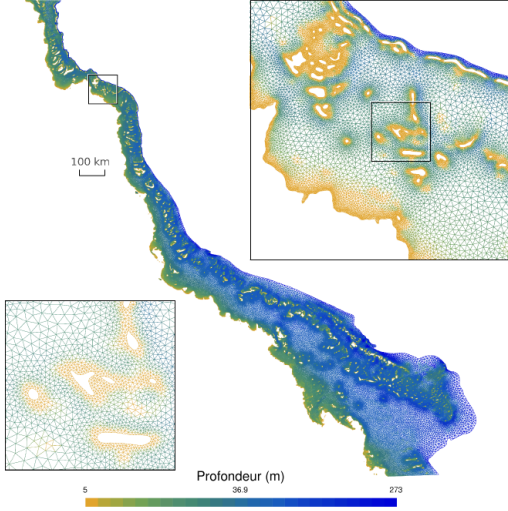
The processes that take place in the flow over the GBR occur over a wide range of scales of motion, from a few metres around small reefs to regional flows over hundreds of kilometres. Satellite imagery and numerical simulations show that small-scale phenomena such as eddies and tidal jets are mainly confined to the neighbourhood of small reefs, islands and passages (Hamner and Hauri, 1981; Wolanski and Hamner, 1988; Wolanski et al., 1988; Deleersnijder et al., 1992; Wolanski et al., 1996), and so have a significant effect on the ecosystem of the GBR. It is therefore essential to simultaneously simulate all scales of motion, as small and large scale processes experience significant interactions (Wolanski et al., 2003c). So when designing the mesh, higher resolution is required in the vicinity of islands and reefs and lower resolution in open waters, where the scales of motion are much larger.

The resolution of the meshes for the GBR and meshes for the domains containing islands (Figure 1.1) must therefore depend on two criteria:

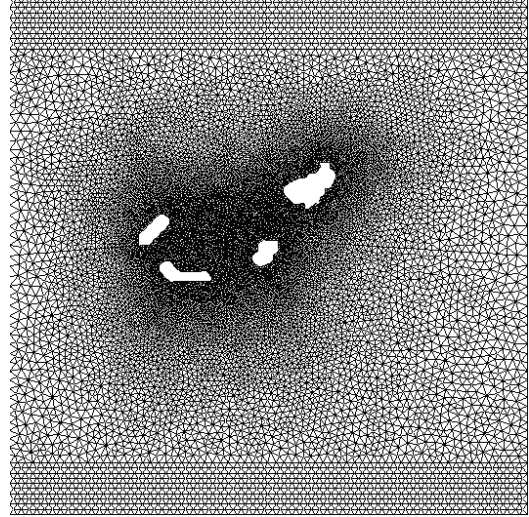
- The Courant-Friedrichs-Lewy condition (CFL condition) for the gravity waves over the whole domain must be satisfied. Essentially this means that the local mesh size has to be equal to the square root of the water depth^[1].
- The local mesh size must depend on the distance to islands and reefs in order cluster mesh nodes in regions where small scale processes are likely to take place. The mesh is refined even more in the vicinity of islands where eddies and tidal jets can be expected^[1].

1.3 Numerical discretization of the SWEs

An approximate solution of the SWEs under the conditions mentioned above is obtained using the finite element method. The finite difference method is not used as it cannot handle unstructured grids. The method used is known as the $P_1^{NC} - P_1$ finite element method and



(c) Fine mesh resolution around islands and course mesh resolution in open waters, image taken from [1]



(d) Fine mesh resolution around islands and open boundaries. Images courtesey of Emmanuel Hartert

Figure 1.1: Model resolution

the solution is calculated using a 3^{rd} order Adams-Bashforth time marching scheme. The main features of these methods are described below.

1.3.1 The $P_1^{NC} - P_1$ finite element formulation

Let's remind ourselves of the equations we wish to solve:

$$\frac{\partial \eta}{\partial t} + \nabla \cdot (H\mathbf{u}) = 0, \quad (1.2)$$

$$\frac{\partial \mathbf{u}}{\partial t} + \mathbf{u} \cdot \nabla \mathbf{u} + f\mathbf{k} \times \mathbf{u} + g\nabla \eta = \frac{1}{H} (\nabla \cdot (\nu H \nabla \mathbf{u})) + \frac{\tau}{\rho H} - \frac{g\|\mathbf{u}\|}{C^2 H} \mathbf{u}, \quad (1.3)$$

where \mathbf{k} is a unit vector in the vertical direction and ∇ is the two-dimensional gradient operator. To use the finite element spatial discretization some notation for our domain, elements and boundaries of elements will need to be introduced. Proceeding as in [3], the domain (call it Ω) is first partitioned into N_E disjoint open elements Ω_e :

$$\bar{\Omega} = \bigcup_{e=1}^{N_E} \bar{\Omega}_e \quad \text{and} \quad \Omega_e \cap \Omega_f = \emptyset \quad \text{for} \quad e \neq f,$$

where $\bar{\Omega}$ is the closure of Ω . Now let $\partial\Omega_e$ be the boundary of each element Ω_e , and let the outward unit normal to $\partial\Omega_e$ be \mathbf{n}_e . Let Γ be the collection of all the interelement boundaries $\Gamma_l = \partial\Omega_e \cap \partial\Omega_f$ with $e > f$ so that:

$$\bar{\Gamma} = \bigcup_{l=1}^{N_\Gamma} \bar{\Gamma}_l \quad \text{and} \quad \Gamma_l \cap \Gamma_m = \emptyset \quad \text{for} \quad l \neq m,$$

where N_Γ is the number of elements in Γ . Each $\Gamma_l \in \Gamma$ is associated with a unique normal vector \mathbf{n} which point from Ω_e to Ω_f . The finite element method uses the weak formulation of equations (1.2) and (1.3). This form is built in such a way that the solution for the elevation is continuous everywhere whereas the solution for the velocity can be discontinuous between elements. It therefore needs constraints to impose the continuity of the velocity between the elements. The weak form of the SWEs, obtained by taking the dot product of equations (1.2) and (1.3) with test functions $\hat{\eta}$ and $\hat{\mathbf{u}}$ respectively, is as follows:

Find $\eta(x, t) \in E$ and $\mathbf{u}(\mathbf{x}, t) \in U$ such that

$$\sum_{e=1}^{N_E} \int_{\Omega_e} \left(\frac{\partial \eta}{\partial t} \hat{\eta} - H \mathbf{u} \cdot \nabla \hat{\eta} \right) d\Omega + \sum_{e=1}^{N_E} \int_{\partial\Omega_e} H \hat{\eta} \mathbf{u} \cdot \mathbf{n}_e d\Gamma = 0 \quad \forall \hat{\eta} \in E, \quad (1.4)$$

$$\begin{aligned} & \sum_{e=1}^{N_E} \int_{\Omega_e} \left(\frac{\partial \mathbf{u}}{\partial t} \cdot \hat{\mathbf{u}} - (\nabla \cdot (\mathbf{u} \hat{\mathbf{u}})) \cdot \mathbf{u} + f(\mathbf{k} \times \mathbf{u}) \cdot \hat{\mathbf{u}} + g \nabla \eta \cdot \hat{\mathbf{u}} - \frac{1}{H} (\nabla \cdot (\nu H \nabla \mathbf{u})) \cdot \hat{\mathbf{u}} \right. \\ & \left. - \frac{\tau}{\rho H} \cdot \hat{\mathbf{u}} + \frac{g \|\mathbf{u}\|}{C^2 H} \mathbf{u} \cdot \hat{\mathbf{u}} \right) d\Omega + \sum_{e=1}^{N_E} \int_{\partial\Omega_e} (\mathbf{u} \mathbf{u} \cdot \mathbf{n}_e) \cdot \hat{\mathbf{u}} d\Gamma + \sum_{l=1}^{N_\Gamma} \int_{\Gamma_l} [\mathbf{u}] \cdot [\mathbf{a}(\hat{\mathbf{u}})] d\Gamma \\ & = 0 \quad \forall \hat{\mathbf{u}} \in U, \quad (1.5) \end{aligned}$$

where $[\mathbf{s}] = \mathbf{s}|_{\Omega_e} - \mathbf{s}|_{\Omega_f}$ is the jump of \mathbf{s} on an interior edge of Γ_l , $\mathbf{s}|_{\Omega_e}$ denotes the restriction of \mathbf{s} on Ω_e , and E and U are suitable function spaces^[3] to which $\hat{\eta}$ and $\hat{\mathbf{u}}$ belong. The function \mathbf{a} satisfies the previously mentioned continuity constraint while maintaining the weak formulation of the differential equations. The function \mathbf{a} satisfies:

$$\mathbf{a}(\hat{\mathbf{u}}) = \begin{cases} \mathbf{u} \cdot \mathbf{n}(\lambda - 1/2) \hat{\mathbf{u}} & \text{on } \Omega_e, \\ \mathbf{u} \cdot \mathbf{n}(\lambda + 1/2) \hat{\mathbf{u}} & \text{on } \Omega_f, \end{cases}$$

where $\lambda \in [-1/2, 1/2]$. The choice of λ selects the type of scheme used. A centred scheme is obtained by choosing $\lambda = 0$ and an upwind momentum advection scheme is obtained

by choosing $\lambda = \frac{1}{2}\text{sign}(\mathbf{u}(\mathbf{x}) \cdot \mathbf{n}(\mathbf{x}))$. Choosing the upwind parametrization that is usually selected (Houston et al., 2000; Hanert et al., 2004), with some standard algebra (Houston et al., 2000; Hanert et al., 2004) the weak formulations (1.4) and (1.5) can be rewritten as:

Find $\eta(x, t) \in E$ and $\mathbf{u}(\mathbf{x}, t) \in U$ such that

$$\begin{aligned} \sum_{e=1}^{N_E} \int_{\Omega_e} \left(\frac{\partial \eta}{\partial t} \hat{\eta} - H \mathbf{u} \cdot \nabla \hat{\eta} \right) d\Omega + \sum_{l=1}^{N_\Gamma} \int_{\Gamma_l} (\langle H \mathbf{u} \cdot \mathbf{n} \rangle [\hat{\eta}] + [H \mathbf{u} \cdot \mathbf{n}] \langle \hat{\eta} \rangle) d\Gamma \\ = 0 \quad \forall \hat{\eta} \in E, \end{aligned} \quad (1.6)$$

$$\begin{aligned} \sum_{e=1}^{N_E} \int_{\Omega_e} \left(\frac{\partial \mathbf{u}}{\partial t} \cdot \hat{\mathbf{u}} - (\nabla \cdot (\mathbf{u} \hat{\mathbf{u}})) \cdot \mathbf{u} + f(\mathbf{k} \times \mathbf{u}) \cdot \hat{\mathbf{u}} + g \nabla \eta \cdot \hat{\mathbf{u}} - \frac{1}{H} (\nabla \cdot (\nu H \nabla \mathbf{u})) \cdot \hat{\mathbf{u}} \right. \\ \left. - \frac{\tau}{\rho H} \cdot \hat{\mathbf{u}} + \frac{g \|\mathbf{u}\|}{C^2 H} \mathbf{u} \cdot \hat{\mathbf{u}} \right) d\Omega + \sum_{l=1}^{N_\Gamma} \int_{\Gamma_l} \langle \mathbf{u} \mathbf{u} \cdot \mathbf{n} \rangle_\lambda \cdot [\hat{\mathbf{u}}] d\Gamma = 0 \quad \forall \hat{\mathbf{u}} \in U, \end{aligned} \quad (1.7)$$

where $\langle s \rangle$ and $\langle s \rangle_\lambda$ are the average and weighted average of \mathbf{s} on the segment Γ_l respectively, i.e.

$$\begin{aligned} \langle \mathbf{s} \rangle &= \frac{1}{2} (\mathbf{s}_{|\Omega_e} + \mathbf{s}_{|\Omega_f}) \\ \langle \mathbf{s} \rangle_\lambda &= (1/2 + \lambda) \mathbf{s}_{|\Omega_e} + (1/2 - \lambda) \mathbf{s}_{|\Omega_f} \end{aligned}$$

A finite element approximation to the solution of equations (1.1) is obtained by replacing η and \mathbf{u} in (1.6) and (1.7) with finite element approximations η^h and \mathbf{u}^h . These approximations belong to finite dimensional spaces $E^h \in E$ and $U^h \in U$. They are:

$$\begin{aligned} \eta \approx \eta^h &= \sum_{i=1}^{N_V} \eta_i \phi_i, \\ \mathbf{u} \approx \mathbf{u}^h &= \sum_{j=1}^{N_S} \mathbf{u}_j \psi_j, \end{aligned}$$

where N_V and N_S represent the number of vertices and number of segments respectively, η_i and \mathbf{u}_j represent elevation and velocity nodal values, and ϕ_i and ψ_j represent the elevation and velocity shape functions associated with a particular node. The nodal values are then computed using the Galerkin procedure, which amounts to replacing $\hat{\eta}$ with ϕ_i and $\hat{\mathbf{u}}$ by $(\psi_j, 0)$ and $(0, \psi_j)$ in equations (1.6) and (1.7) respectively, for $1 \leq i \leq N_V$ and $1 \leq j \leq N_S$

(Hanert et al., 2005).

The next section describes the shape functions ϕ_i and ψ_j and certain properties of these functions can simplify the variational form.

1.3.2 The non-conforming mixed $P_1^{NC} - P_1$ finite element pair

The $P_1^{NC} - P_1$ finite element pair is made up of the linear conforming (P_1) and the linear non-conforming (P_1^{NC}) shape functions (see figure 1.2). In this triangulation, the nodal values for the elevation lie on the vertices of an element while the nodal values of the velocity lie on the midpoints of the segments (see figure 1.3).

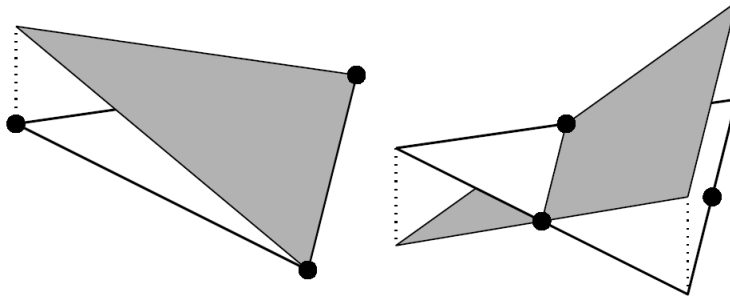


Figure 1.2: The linear conforming (left) and linear non-conforming (right) shape functions, image taken from [3]

With this choice of shape functions, the discrete elevation field is everywhere continuous whereas the discrete velocity field is only continuous across element boundaries at mid-segment nodes and discontinuous everywhere else around a triangle boundary.

A major advantage of the P_1^{NC} shape functions is their orthogonality property (Hanert et al., 2005):

$$\int_{\Omega} \psi_p \psi_q \, d\Omega = \frac{A_q}{3} \delta_{pq}$$

where A_q is the area of support of ψ_q and δ_{pq} is the Kronecker delta. This unusual property increases the computational efficiency of the numerical model (Hanert et al., 2005). To further improve the efficiency the following approximation in the variational formulation

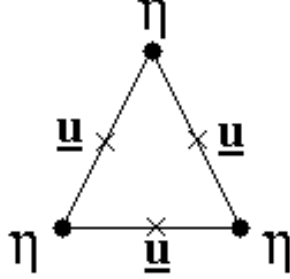


Figure 1.3: Position of elevation and velocity nodes on an element

(1.6) and (1.7) is performed:

$$\underbrace{\int_{\Gamma_l} \langle H \mathbf{u}^h \cdot \mathbf{n} \rangle [\phi_i] d\Gamma}_{=0} + \int_{\Gamma_l} [H \mathbf{u}^h \cdot \mathbf{n}] \langle \phi_i \rangle d\Gamma \approx 0. \quad (1.8)$$

(Note that where previously $H = h + \eta$, in (1.8) η has been replaced with the finite element approximation η^h giving $H = h + \eta^h$).

The first term in (1.8) vanishes because of the continuity across the P_1 shape functions - there is no jump in the elevation shape function, i.e. $[\phi_i] = 0$. The second term is neglected in order to guarantee mass conservation at the cost of a small loss of accuracy (Hanert et al., 2005). An approximation for the product of \mathbf{u}^h with f is also made to the variational formulation:

$$\int_{\Omega_e} f(\mathbf{k} \times \mathbf{u}^h) \psi_j d\Omega = \int_{\Omega_e} f \sum_{i=1}^{N_S} \psi_i \psi_j d\Omega \approx \int_{\Omega_e} \underbrace{\sum_{i=1}^{N_S} f_i(\mathbf{k} \times \mathbf{u}_i)}_{(f \mathbf{k} \times \mathbf{u})^h} \psi_i \psi_j d\Omega, \quad (1.9)$$

where f_i represents the value of the Coriolis parameter at a velocity node. Since f varies smoothly throughout the domain, using the approximation given in equation (1.9) only has a small effect on the accuracy of the solution while greatly simplifying the algebra (Hanert et al., 2005).

With both of these approximations the variational (or weak) formulation for the discretized equations reads:

$$\sum_{e=1}^{N_E} \int_{\Omega} \left(\frac{\partial \eta^h}{\partial t} \phi_i - H \mathbf{u}^h \cdot \nabla \phi_i \right) d\Omega = 0 \quad \text{for } 1 \leq i \leq N_V, \quad (1.10)$$

$$\begin{aligned} \sum_{e=1}^{N_E} \int_{\Omega} \left(\frac{\partial \mathbf{u}^h}{\partial t} \psi_j - \mathbf{u}^h \nabla \cdot (\mathbf{u}^h \psi_j) + g \nabla \eta^h \psi_j - \frac{1}{H} (\nabla \cdot (\nu H \nabla \mathbf{u})) \cdot \psi_j - \frac{\tau}{\rho H} \cdot \psi_j \right. \\ \left. + \frac{g \|\mathbf{u}\|}{C^2 H} \mathbf{u} \cdot \psi_j \right) d\Omega + \sum_{l=1}^{N_{\Gamma}} \int_{\Gamma_l} \langle \mathbf{u}^h \mathbf{u}^h \cdot \mathbf{n} \rangle_{\lambda} [\psi_j] d\Gamma = 0 \quad \text{for } 1 \leq j \leq N_S. \end{aligned} \quad (1.11)$$

In addition to being discretized in space, the SWEs must also be discretized with respect to time. The next section briefly outlines the time integration scheme used by the model.

1.3.3 Time integration scheme

The model uses the Adams-Bashforth 3 (AB3) time integration scheme to solve the variational form of the SWEs. The first step in this scheme entails rearranging our differential equations (1.10) and (1.11) to the following form (for ease of notation the temporal discretizations of (1.2) and (1.3) are presented):

$$\frac{\partial \eta}{\partial t} = F_{\eta}(\eta, \mathbf{u}, t), \quad (1.12)$$

$$\frac{\partial \mathbf{u}}{\partial t} = F_{\mathbf{u}}(\eta, \mathbf{u}, t), \quad (1.13)$$

Then for a given time step $\Delta t = t^{n+1} - t^n$, the AB3 discretization of equations (1.12) and (1.13) reads:

$$\begin{aligned} \frac{\eta^{n+1} - \eta^n}{\Delta t} &= \frac{1}{12} (23F_{\eta}^n - 16F_{\eta}^{n-1} + 5F_{\eta}^{n-2}), \\ \frac{\mathbf{u}^{n+1} - \mathbf{u}^n}{\Delta t} &= \frac{1}{12} (23F_{\mathbf{u}}^n - 16F_{\mathbf{u}}^{n-1} + 5F_{\mathbf{u}}^{n-2}), \end{aligned}$$

where

$$F_\eta^n = -\nabla \cdot (H\mathbf{u}^n),$$

and

$$F_{\mathbf{u}}^n = -\mathbf{u}^n \cdot \nabla \mathbf{u}^n - f\mathbf{k} \times \mathbf{u}^n - g\nabla \eta^n + \frac{1}{H} (\nabla \cdot (\nu H \nabla \mathbf{u}^n)) + \frac{\tau}{\rho H} - \frac{g\|\mathbf{u}^n\|}{C^2 H} \mathbf{u}^n.$$

Rearranging again to leave η^{n+1} and \mathbf{u}^{n+1} on the left hand sides of our equations gives:

$$\begin{aligned} \eta^{n+1} &= \eta^n + \frac{\Delta t}{12} (23F_\eta^n - 16F_\eta^{n-1} + 5F_\eta^{n-2}), \\ \mathbf{u}^{n+1} &= \mathbf{u}^n + \frac{\Delta t}{12} (23F_{\mathbf{u}}^n - 16F_{\mathbf{u}}^{n-1} + 5F_{\mathbf{u}}^{n-2}). \end{aligned}$$

As η^n and \mathbf{u}^n are vectors taking values over the whole domain, we obtain the following matrix system of linear equations:

$$\begin{pmatrix} A & 0 \\ 0 & B \end{pmatrix} \begin{pmatrix} U^{n+1} \\ H^{n+1} \end{pmatrix} = \begin{pmatrix} R_U \\ R_H \end{pmatrix} \quad (1.14)$$

where U^{n+1} and H^{n+1} are the values of η and \mathbf{u} on the mesh nodes, defined as

$$U^{n+1} = \begin{pmatrix} u_i \\ v_i \end{pmatrix} \quad \text{and} \quad H^{n+1} = (\eta_j),$$

where $1 \leq i \leq N_S$ and $1 \leq j \leq N_V$. The matrix A on the left hand side of equation (1.14) is diagonal. In terms of computation efficiency this is a major advantage as it means that we do not have to invert any large matrices or ‘lump’ any terms. The matrix B is not diagonal, and so here the ‘lumping’ technique is required to put the off diagonal terms onto the diagonal. With both the spatial and time discretization the elements of the matrices A and B are:

$$A_{ij} = \sum_e \int_{\Omega_e} \psi_i \psi_j \, d\Omega \quad (1.15)$$

$$B_{ij} = \left(\sum_e \int_{\Omega_e} \phi_i \phi_k \, d\Omega \right) \delta_{ij}. \quad (1.16)$$

Equation (1.16) can be interpreted as adding all of the terms $\int_{\Omega_e} \phi_i \phi_k \, d\Omega$ to entry B_{ij} when $i = j$.

Chapter 2

Simulation of the transport of water-borne larvae

Now that an understanding of a model to simulate the flow around reefs has been obtained, the release of particles from reefs can start to be considered. The aim of this study is to develop an algorithm that will simulate the dispersion of coral eggs (particles) produced by coral reefs. In the simulation, these particles will be released from islands in a square domain. The flow through this domain is produced by forcings applied to the two open boundaries parallel to the x-axis. Once the algorithm is in place, the connectivity between islands can then be investigated. The stages of development to implement such an algorithm are as follows:

- Choose an advection-diffusion algorithm - will the Eulerian or Lagrangian approach to track the coral eggs be used?
- Integration of the advection-diffusion algorithm with the model - what work must be done before the model can be built?
- Testing of the advection-diffusion algorithm - the algorithm must first be tested and validated on a simple case to ensure that it works.
- Implementation of the model on the domains of interest - on the domains containing two and four islands.

This chapter goes into detail about each of these stages and gives the results of the simple Stommel test case.

2.1 Choosing an advection-diffusion algorithm

2.1.1 Eulerian or Lagrangian?

The tracking of a group or cluster of particles in a flow could be done by either:

- considering a group of particles as a passive tracer and monitor its concentration c (Eulerian formulation), or
- following each particle individually and, given its velocity, update its position at each time step (Lagrangian formulation).

In a 2-D approach, the concentration c of a passive tracer is governed by the Eulerian equation

$$\frac{\partial(hc)}{\partial t} = -\nabla \cdot (\mathbf{u}hc - hk\nabla c) \quad (2.1)$$

where t , $h(> 0)$ and $k(> 0)$ denote time, water depth and the horizontal diffusivity respectively ([6]), and \mathbf{u} is the depth averaged velocity. According to [6], accurate numerical simulations of (2.1) are not easy to obtain due to difficulty in finding accurate Eulerian discretizations of the advective operator $-\nabla \cdot (\mathbf{u}hc)$. Thus the Lagrangian algorithm is often used to predict the fate of water-borne propagules near coral reefs, for example sewage, coral eggs and larvae, plankton, fish and crown-of-thorn starfish (Sammarco & Andrews 1988, 1989, Wolanski et al., 1989, 1997, Black et al. 1990, 1991, Dight et al. 1990, Oliver et al. 1992, Black 1993), [6]. For this reason, this study will use the Lagrangian approach. The Lagrangian algorithm, as given in [6], reads:

At time $t_n = n\Delta t$ ($n = 1, 2, 3, \dots$), where Δt is a suitable time increment, the position $\mathbf{x}_n = (x_n, y_n)$ of a water-borne propagule is updated by:

$$\mathbf{x}_{n+1} = \mathbf{x}_n + \mathbf{v}\Delta t + \frac{\mathbf{R}_n}{\sqrt{r}}\sqrt{2k\Delta t} \quad (2.2)$$

where the velocity \mathbf{v} is set to \mathbf{u} , \mathbf{R}_n is a vector of zero mean random numbers with variance r and k is the horizontal diffusivity. It is believed that the concentration of particles, which may be calculated from their positions, tends to be equivalent to the solution of the Eulerian advection-diffusion equation (2.1)[6]. However, if h or k are not constant, i.e. they vary in space, then this assumption becomes incorrect. The last section addresses this issue and suggests an alternative algorithm to correct it. This study will use the Lagrangian algorithm and test different the values for the diffusivity parameter k .

2.2 Integration of the advection-diffusion algorithm with the model

Before the advection-diffusion model can be written, some work needs to be done in order to gain access to the correct values of velocity calculated by the model of the flow. The velocity nodes are located on the element mid-segments (see Figure 1.3). This throws up two problems: firstly, given the cartesian coordinates, the element a point lies in needs to be found - the model does not provide a function for this; secondly, the value of the velocity is needed at a point, not the value of the velocity on the three segments of the containing element.

This section describes a number of methods to solve the first problem, and explains how the P_1^{NC} and P_1 weight functions are used to solve the second.

2.2.1 The ‘point in a triangle’ test

There are a number of ways to check if a point, call it point P , is in a triangle (or an element!). The methods described below have been taken from [11].

A common way is to find the vectors connecting P to the vertices of the triangle and sum the angles between those vectors. If the sum is equal to 2π then P is inside the triangle, otherwise not.

This method works but is very slow. Two faster methods are the ‘same side technique’ and the even faster ‘Barycentric technique’.

The ‘same side technique’

Consider a triangle with vertices A , B and C . The lines AB , BC , and CA each split 2-dimensional space in half, with one of those halves being entirely outside the triangle (see Figure 2.1). For a point P to be inside the triangle ABC , it must be below AB and left of BC and right of AC . If any one of these tests fails we stop early as we know that our point P cannot be inside the triangle. The implementation of these tests requires a process to determine whether or not P lies on the correct side of the line. This process is as follows:

- Assume another point Q lies outside of the triangle (Figure 2.2). Taking the cross

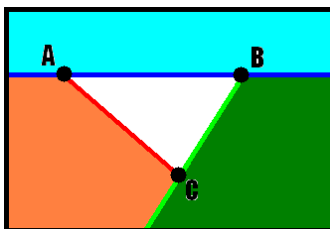


Figure 2.1: Each edge of a triangle splits 2-D space in half, image from [11]

product of the vectors $(B - A)$ and $(P - A)$ gives a vector pointing in to the page. Conversely, taking the cross product of $(B - A)$ and $(Q - A)$ gives a vector pointing out of the page.

- Moreover, taking the cross product of $(B - A)$ with the vector from A to any point above the line AB results in a vector pointing out of the page, while using any point below AB produces a vector pointing into the page. So all that is needed to distinguish which side of a line a point lies on is the appropriate cross product.
- Now all that is needed to be done is to work out which direction the cross product should point in. To calculate this, a reference point that is always on one side of the line is needed. The third vertex of the triangle will do nicely.

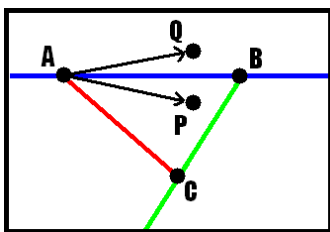


Figure 2.2: How do we mathematically determine which point is in the triangle? Image from [11]

Any point P where $(B - A) \times (P - A)$ does not point in the same direction as $(B - A) \times (C - A)$ isn't inside the triangle. If the cross products do point in the same direction, then P needs to be tested with the other lines as well. If the point is on the same side of AB as C and is also on the same side of BC as A and on the same side of CA as B , then it is in the triangle.

The Barycentric technique

The Barycentric technique is another conceptually simple technique for determining whether

a point is in a triangle or not, it requires slightly more algebra than the ‘same side technique’ but computes faster. This is the technique that will be employed in the model.

The three points of a triangle define a plane in space. Let A be the origin of this plane. Through combinations of the vectors $(B - A)$ and $(C - A)$ any point in the plane can be reached. In particular, the point P can be described as

$$P = A + u(B - A) + v(C - A)$$

If u or v is greater than one or less than zero then the point is outside of the triangle as it is too far from A in one of the directions $\pm(B - A)$ or $\pm(C - A)$. Furthermore if $u + v > 1$ then the point is outside of the triangle as the combination $A + u(B - A) + v(C - A)$ has taken the point past edge BC . If any of these tests fail then the point cannot be in this triangle. P is easily found given u and v , but what is needed is to find u and v given P . The position of P is given above as one equation in two unknowns. Two equations in two unknowns are produced as follows.

For ease of notation let $(P - A) = V_0$, $(B - A) = V_1$ and $(C - A) = V_2$ so that

$$P - A = u(B - A) + v(C - A)$$

becomes

$$V_0 = uV_1 + vV_2.$$

To get two equations in two unknowns, take the dot product of both sides with V_1 and then with V_2 to give

$$\begin{aligned} V_0 \cdot V_1 &= u(V_1 \cdot V_1) + v(V_2 \cdot V_1) \\ V_0 \cdot V_2 &= u(V_1 \cdot V_2) + v(V_2 \cdot V_2). \end{aligned}$$

Solving this pair of simultaneous equations gives us u and v :

$$\begin{aligned} u &= \frac{(V_2 \cdot V_2)(V_0 \cdot V_1) - (V_2 \cdot V_1)(V_0 \cdot V_2)}{(V_2 \cdot V_2)(V_1 \cdot V_1) - (V_2 \cdot V_1)(V_1 \cdot V_2)} \\ v &= \frac{(V_1 \cdot V_1)(V_0 \cdot V_2) - (V_1 \cdot V_2)(V_0 \cdot V_1)}{(V_2 \cdot V_2)(V_1 \cdot V_1) - (V_2 \cdot V_1)(V_1 \cdot V_2)}. \end{aligned}$$

So given the vertices of an element and the position of a point P , whether or not P lies in the element is worked out by simply calculating u and v as above and checking whether or not $u, v \in [0, 1]$ and $u + v < 1$.

2.2.2 Using the P_1 and P_1^{NC} weight functions to determine velocity at a point

In order to use the Lagrangian algorithm it must be possible to calculate the velocity at any point in the domain. The velocity is prescribed on the mid-segments of the elements. Now that the element in which a point lies can be determined, the three values of velocity stored on the element segments are accessible. Since the element size is quite large (element sizes range from 10m to 500m) compared to the distance a particle will move in a single time step, calculating the velocity at a point is not as simple as taking a simple average of these three velocities. Recall that the finite element approximation to the velocity is

$$\mathbf{u}(x, y, t) \approx \mathbf{u}^h(x, y, t) = \sum_{i=0}^2 \mathbf{u}_i \psi_i(x, y)$$

where the \mathbf{u}_i are the velocities stored on the segments and ψ_i are the P_1^{NC} shape functions. These shape functions are related to the P_1 shape functions ϕ_i by

$$\psi_i(x, y) = 1 - 2\phi_i(x, y)$$

where the P_1 shape functions are given by

$$\phi_i = \alpha_i x + \beta_i y + \gamma_i. \tag{2.3}$$

Diagrams of these shape functions are given in Figures 1.2 and 2.3. So to find the velocity at a point (x, y) , the coefficients α_i , β_i and γ_i are needed. The values of ϕ_i on the nodes of an element are known: if \mathbf{x}_0 , \mathbf{x}_1 and \mathbf{x}_2 are the nodes of element p then

$$\phi_i(\mathbf{x}_j) = \begin{cases} 0 & i \neq j \\ 1 & i = j \end{cases}$$

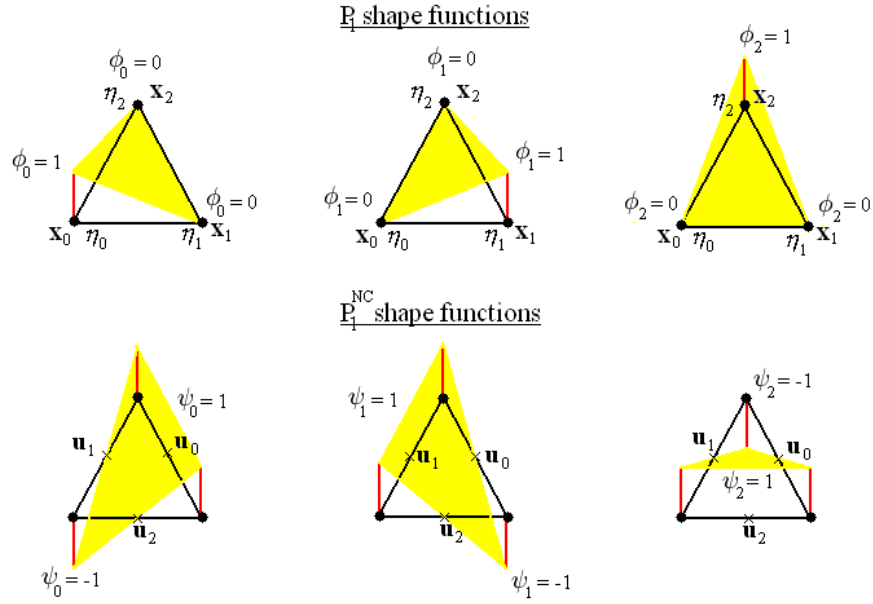


Figure 2.3: Shape functions

and so for each i there are three equations in three unknowns. For example for $i = 0$:

$$\begin{aligned}\phi_0(\mathbf{x}_0) &= 1 = \alpha_0 x_0 + \beta_0 y_0 + \gamma_0 \\ \phi_0(\mathbf{x}_1) &= 0 = \alpha_0 x_1 + \beta_0 y_1 + \gamma_0 \\ \phi_0(\mathbf{x}_2) &= 0 = \alpha_0 x_2 + \beta_0 y_2 + \gamma_0.\end{aligned}$$

Solving these simultaneous equations, for $i = 0$ for example, gives:

$$\begin{aligned}\alpha_0 &= \frac{y_1 - y_2}{(x_0 - x_2)(y_1 - y_2) + (x_2 - x_1)(y_0 - y_2)}, \\ \beta_0 &= \frac{x_2 - x_1}{(x_0 - x_2)(y_1 - y_2) + (x_2 - x_1)(y_0 - y_2)}, \\ \gamma_0 &= \frac{x_1 y_2 - x_2 y_1}{(x_0 - x_2)(y_1 - y_2) + (x_2 - x_1)(y_0 - y_2)},\end{aligned}$$

$\alpha_1, \alpha_2, \beta_1, \beta_2, \gamma_1$ and γ_2 are found in the same way. A general form for α_i, β_i and γ_i can be written using the modulo operation:

$$\begin{aligned}\alpha_i &= \frac{y_{(i+1)|3} - y_{(i+2)|3}}{(x_{i|3} - x_{(i+2)|3})(y_{(i+1)|3} - y_{(i+2)|3}) + (x_{(i+2)|3} - x_{(i+1)|3})(y_{i|3} - y_{(i+2)|3})}, \\ \beta_i &= \frac{x_{(i+2)|3} - x_{(i+1)|3}}{(x_{i|3} - x_{(i+2)|3})(y_{(i+1)|3} - y_{(i+2)|3}) + (x_{(i+2)|3} - x_{(i+1)|3})(y_{i|3} - y_{(i+2)|3})}, \\ \gamma_i &= \frac{x_{(i+1)|3} * y_{(i+2)|3} - x_{(i+2)|3} * y_{(i+1)|3}}{(x_{i|3} - x_{(i+2)|3})(y_{(i+1)|3} - y_{(i+2)|3}) + (x_{(i+2)|3} - x_{(i+1)|3})(y_{i|3} - y_{(i+2)|3})},\end{aligned}$$

where $(i+k)|3$ stands for $(i+k)\bmod 3$. In this general form the ϕ_i s can be calculated using a single function that takes the position of a point (or particle) as an argument. From this the ψ_i s can be calculated and hence the velocity at any point in the domain.

2.2.3 Construction of the diffusion term

The Lagrangian algorithm consists of an advective and a diffusive term. So far the steps to implementing advective term $\mathbf{v}\Delta t$ (where \mathbf{v} is set to \mathbf{u} as in equation (2.1)) have been considered. The construction of the diffusive term $\frac{\mathbf{R}_n}{\sqrt{r}}\sqrt{2k\Delta t}$ requires

- a vector $\mathbf{R}_n = (R_x, R_y)$ of zero mean random numbers taking values in $[-1, 1]$,
- calculation of the variance of these random numbers
- a choice for the diffusivity parameter k .

The components of \mathbf{R}_n are obtained using the `srand` and `rand` functions defined in the standard C++ library. Two random numbers R_1 and R_2 between 0 and 200 are produced and translated to the interval $[-1, 1]$ using the formulae

$$\begin{aligned}R_x &= R_1/100 - 1, \\ R_y &= R_2/100 - 1,\end{aligned}$$

giving 201 possible values for each of R_x and R_y .

The variance r of these 201 random variables, call them x_k , is calculated using the standard formula:

$$r = \sum_{k=0}^{k=200} (x_k - \bar{x})^2 = 0.33667.$$

As for the choice of diffusivity parameter k , a range of values will be tested. The model only allows particles to be released from a finite number of points around the islands, however many particles can be released from each point. In order to find the best value to represent the dispersion of coral eggs in the flows through the two and four island domains, values of 0.5, 1.0 and 2.0 (as used in [6]) up to much larger values of about $50.0\text{m}^2\text{s}^{-1}$ will be tested.

2.3 Testing the advection diffusion algorithm

In order to test the advection diffusion algorithm, the model is run on the Stommel test case. The Stommel model simulates a wind driven circulation in a closed lake or basin. The domain of computation is the interval $[0, L] \times [0, L]$ where $L = 10^6\text{m}$. The physical parameters are given in the table below and the wind field is defined by the following expression:

$$\tau^n = \tau_0 \begin{pmatrix} \cos\frac{\pi y}{2} \\ 0 \end{pmatrix},$$

where $\tau_0 = 0.2\text{Nm}^{-2}$. Initially the flow and the elevation are set to zero.

Parameter	Value
f_0	10^{-4}s^{-1}
g	$10\text{m}^2\text{s}^{-1}$
γ	10^{-6}s^{-1}
ρ	1000kgm^{-3}
h	100m

The velocity and elevation fields produced by the model for this test case are given in Figures 2.4 and 2.5. A particle released into the flow in this model should follow the streamlines of the flow. A plot of the energy in the system against the number of time steps tells us that the system becomes stable after about 3,000,000 time steps (see Figure 2.6). At this point the streamlines will form a closed loop, so the particles should be circulating the domain along the same paths over and over again. Indeed, Figure 2.7 shows that a particle released into the domain on the first time step slowly spirals inward toward the centre while the pathlines get closer and closer together until they are almost closed.

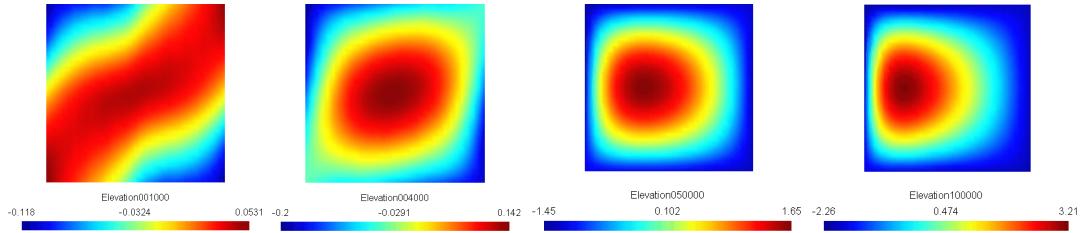


Figure 2.4: Stommel elevation fields at various time steps

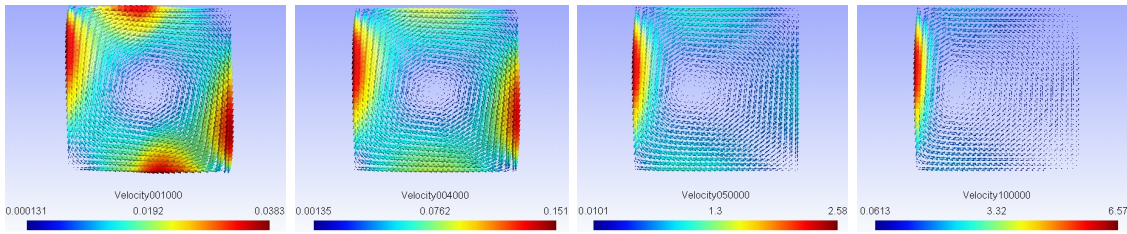


Figure 2.5: Stommel velocity fields at various time steps

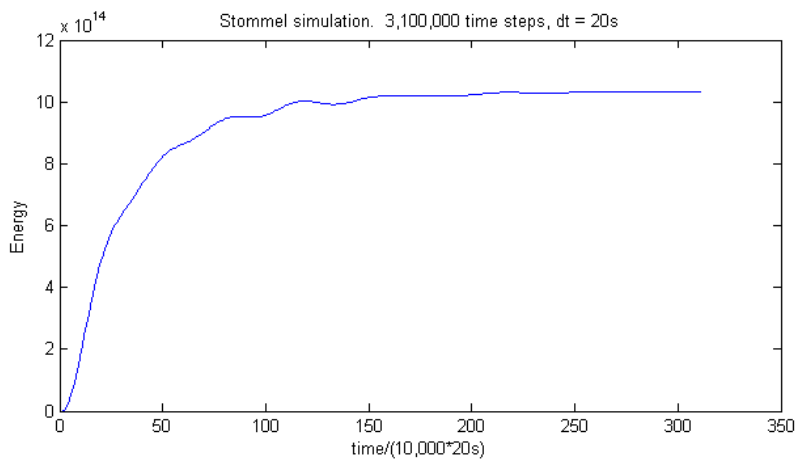


Figure 2.6: Energy in the Stommel simulation

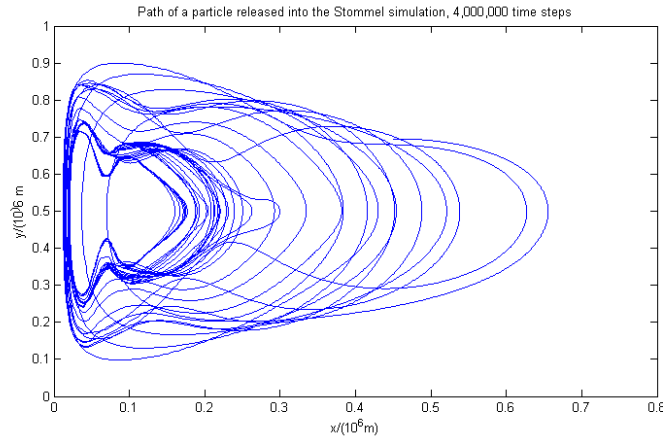


Figure 2.7: A particle released into the Stommel simulation

The particles are behaving as expected and so the model can be considered as validated and the more complicated domains can be investigated.

2.4 Tracking coral eggs from islands

To track coral eggs from the islands, six points roughly spaced around each island are chosen to release coral eggs from. These points are saved in a file and loaded by the model. From these points many coral eggs can be released.

The elevation and velocity fields for the two and four island domains for various time steps are given in Figures 2.8 and 2.9. But for how long should the coral eggs be tracked for? How much time should they spend in the water column before they are able to attach to an island or reef?

Information on the dispersal distances of various water-borne propagules is given in [17]. Figure 2.11 gives these dispersal distances. The organisms of interest are the three species of coral: *Balanophyllia elegans*, *Acroporids* and *Pocilloporids*. The dispersal distances alone are evidence to suggest that these propagules may not actually leave the vicinity of the islands in this study (the element sizes are between 10 and 500m while dispersal distances could be less than 0.6km). Indeed, in a previous study, the Helix experiments on the Great Barrier Reef (Sammarco et al., 1989), significant settlement of coral larvae was only seen

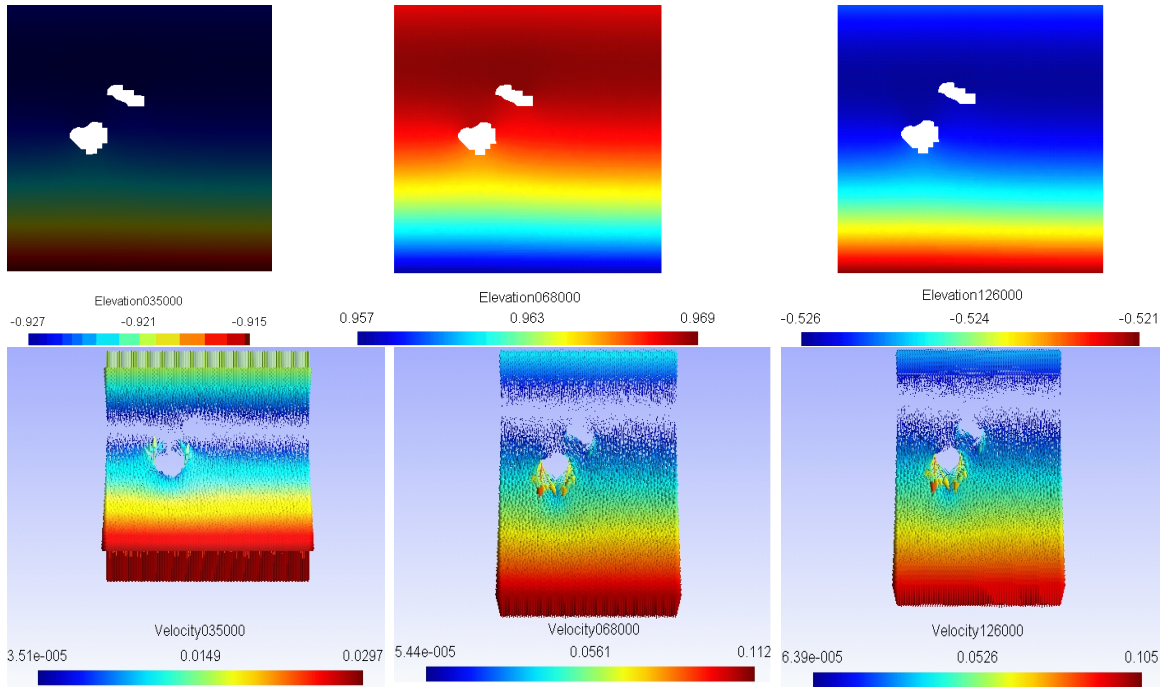


Figure 2.8: Elevation and flow over the two island domain

within several hundred metres of the reef.

Frequently researchers make the simplifying assumption that propagules are dispersed passively by currents^[17]. In [17] actual dispersal distances we compared with dispersal distances that different studies could have found. Figure 2.10 is taken from [17], it gives the dispersal distance of propagules with a line showing what the dispersal distances would have been if they were dispersing passively at a mean current speed of 10cm/s. All of the data points but two of the species fell below the line. It was found that the current speeds in the area where these two species were dispersing were around 30cm/s (*Perna perna* dispersing in the Gulf of Mexico and *Cymatium parthenopeum* in the Atlantic Equatorial current)^[17]. If this current speed was used to estimate the passive dispersal distance then both species would disperse shorter distances than they would if they were dispersing passively.

Included in the plot in Figure 2.10 is the dispersal distance for the larvae of the coral species *Balanophyllia elegans* (A). This type of propagule had the shortest dispersal distance compared to the theoretical passive dispersal distance. This comparison strongly suggests that propagules released from corals are not entirely passive organisms.

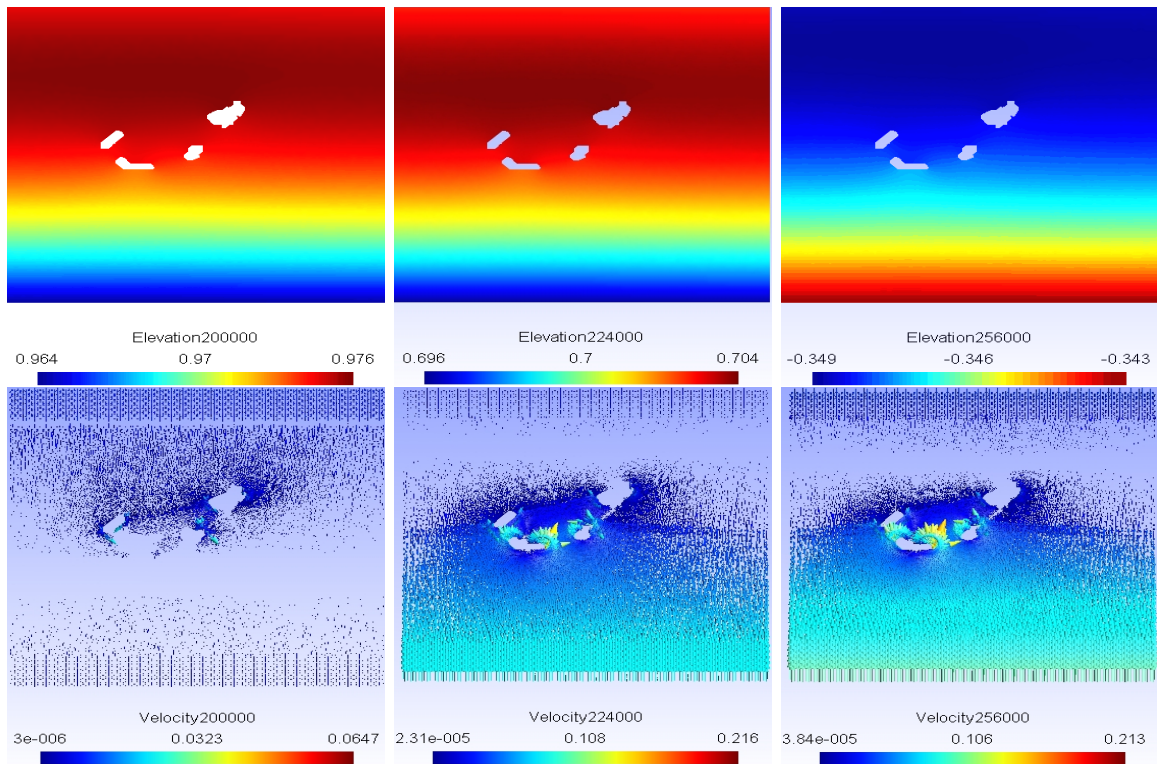


Figure 2.9: Elevation and flow over the four island domain

So if coral larvae are not completely passive and can somehow ‘swim’ toward an island or reef, how can this be modelled?

The initial step in logic taken toward modelling this phenomenon was to consider a radius around each island and decide that once a propagule was inside that radius it could ‘see’ the island and would swim towards it. Any particle inside of that radius would be considered to be settled on that island. Figure 2.12 shows the radii chosen for both the two and four island domains.

The problem with this is that the particles start within these radii, and it is no use to assume that the propagules all attach to the parent reef!

The next step was to introduce a time after which a propagule can settle on an island - the dispersal times for *Balanophyllia elegans*, *Acroporids* and *Pocilloporids* would seem good choices for this! So after a certain dispersal time, if a particle is found within a certain

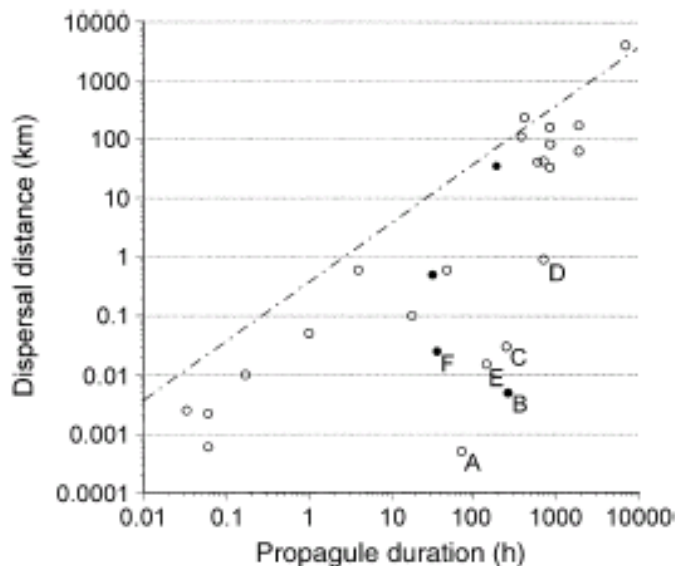


Figure 2.10: A log/log plot of propagule duration vs. dispersal distance. Taken from [17].

radius of an island, the Lagrangian algorithm is no longer implemented, and so the particle is assumed to have settled on that island. For the remaining time steps, particles not within a certain radius of an island are still free to move with the currents, but as soon as one enters one of these radii the algorithm stops for that particle and it is assumed to have settled on the island. The corresponding entry in the final connectivity matrix will refer to the island the particle has settled on and the ‘parent island’ it was released from.

This is all very well, but Figure 2.11 gives different dispersal times for different types of species of coral larvae. To get an idea of why it is important to model different species of coral larvae, compare the reproductive processes of *Balanophyllia elegans* corals and the *Montastrea cavernosa* corals:

- In *Balanophyllia elegans* corals the eggs are fertilized in the mother’s gastrovascular cavity and develop to planula larvae there. The planulae larvae usually settle within 10 cm of the parent^[19].
- The great star corals, *Montastrea cavernosa*, have separate male and female colonies. Male cavernosa star corals discharge their sperm in gushes that resemble puffs of smoke, while female corals release tiny spherical egg sacs^[20]. The water becomes

Estimates of propagule duration and mean realized dispersal distance.

Organism (data source)	Dispersing stage	Duration	Realized dispersal distance (mean)	References
Algae				
<i>Postelsia palmaeformis</i> (E)	spores		3 m	11, 36
<i>Enteromorpha</i> (E)	spores	8 d	35 km	1, 22, 50
<i>Macrocystis pyrifera</i> (E)	spores	32 h	10–40 m	2, 41
<i>Prorygophora californica</i> (E)	spores	32 h	500 m	41
<i>Ectocarpus siliculosus</i> (E)	spores		≥4 km	41
<i>Colpomenia peregrina</i> (E)	spores		<3 m	47
<i>Codium fragile</i> spp. <i>tomentosoides</i> (I)	vegetative fragments, floating		12 km	6
<i>Caulerpa taxifolia</i> (I)	vegetative fragments, bottom		0.5 km	30
<i>Sargassum muticum</i> (E)	germlings	<25 d	<5 m	3, 13
<i>Sargassum muticum</i> (I)	vegetative fragments, floating		28 km (S. English Channel) <90 km (Atlantic coast of Europe) 10–13 km (Mediterranean coast of Europe) 43 km (Baja California)	9, 15, 25
Corals				
<i>Balanophyllia elegans</i> (E)	demersal planula, nonfeeding	3 d	0.1–0.5 m	16
Acroporids (E)	pelagic planula, nonfeeding	24–72 h	≤0.6 km	42
Pocilloporids (E)	brooded planula, nonfeeding	4 hr	≤0.6 km	42
Tunicates				
<i>Didemnum molle</i> (B)	tadpole, nonfeeding	<10 min–2 h	<50 m	33, 34
<i>Diplosoma similis</i> (B)	tadpole, nonfeeding	3.8 ± 2.6 min	2.2 ± 1.8 m	44, 45
<i>Lissoclinum patella</i> (B)	tadpole, nonfeeding	<10 min	<10 m	35
<i>Podoclavella moluccensis</i> (B)	tadpole, nonfeeding	<2 min	<2.5 m	10
<i>Botrylloides</i> sp. (B)	tadpole, nonfeeding	3.6 min	0.6 m (nonfeeding)	49
<i>Botryllus schlosseri</i> (E)	tadpole, rafting tadpole, nonfeeding		225 m (rafting) <1 m	17
Bryozoans				
<i>Bugula neritina</i> (E)	pelagic, nonfeeding	5 min–36 h	<100 m	24
Mollusks				
<i>Cymatium parthenopeum</i> (D)	veliger, feeding	293 d	4400 km	43
<i>Littorina littorea</i> (I)	veliger, feeding	30 d	42 ± 40 km	4, 5, 46, 48
<i>Haliotis rubra</i> (E)	veliger, nonfeeding	6 d	<15 m	38
<i>Ensis directus</i> (I)	veliger, feeding	16 d	111 km	23, 27
<i>Perna perna</i> (I)	veliger, feeding	15–20 d	235 km	21
Crustaceans				
<i>Elminius modestus</i> (I)	pelagic, feeding	17–34 d	41 ± 33 km	8
<i>Alpheus immaculatus</i> (E)	pelagic, feeding	7–14 d	30 m	26
<i>Hemigrapsus penicillatus</i> (I)	pelagic, feeding	16–55 d	160 km	32
<i>Hemigrapsus sanguineus</i> (I)	pelagic, feeding	16–55 d	33 km	14, 29
<i>Carcinus maenas</i> (I)	pelagic, feeding	80 d	173 ± 161 km (west coast of North America) 63 km (east coast North America)	7, 18, 19, 31
Fish				
<i>Lutjanus kasmira</i> (I)	pelagic, feeding	25–47 d	33–130 km	12, 39, 40
<i>Oligocottus maculosus</i> (B, D)	pelagic, feeding	30 d	<1 km	28, 37
Higher plants				
<i>Zostera japonica</i> (I)	seeds, juvenile plants		6 km	20

Notes: References are listed at the end of the table. Data sources for the dispersal-distance estimates are experimental studies (E), observations of dispersing larvae (B), observations on the distribution of larvae (D), and studies that followed the spread of introduced species (I). The data for larval duration came from either laboratory rearing experiments or observations of dispersing larvae. Larval duration has not been measured in *Hemigrapsus penicillatus*. The value used assumes that it is the same as in *Hemigrapsus sanguineus*.

References: 1, Amsler and Searles (1980); 2, Anderson and North (1966); 3, Andrew and Viejo (1998); 4, Bequaert (1943); 5, Brenchley and Carlton (1983); 6, Carlton and Scanlon (1985); 7, Chew (1998); 8, Crisp (1958); 9, Critchley et al. (1983);

Figure 2.11: Table of dispersal distances for different propagules, taken from [17].

10, Davis and Butler (1989); 11, Dayton (1973); 12, E. Demartini (*personal communication*); 13, Deysher and Norton (1982); 14, Epifanio et al. (1998); 15, Espinoza (1990); 16, Gerrodette (1981); 17, Grosberg (1987); 18, Grosholz and Ruiz (1995); 19, Grosholz and Ruiz (1996); 20, Harrison and Bigley (1982); 21, Hicks and Tunnell (1995); 22, Jones and Barb (1968); 23, Kenchington et al. (1998); 24, Keough and Chernoff (1987); 25, Knoepffler-Peguy et al. (1985); 26, Knowlton and Keller (1986); 27, Luczak et al. (1993); 28, Mariave (1986); 29, McDermott (1998); 30, Meinesz et al. (1993); 31, Miller (1996); 32, Noel et al. (1997); 33, Olson (1983); 34, Olson (1985); 35, Olson and McPherson (1987); 36, Paine (1979); 37, Pfister (1997); 38, Prince et al. (1987); 39, Randall (1987); 40, Randall et al. (1993); 41, Reed et al. (1988); 42, Sammarco and Andrews (1989); 43, Scheltema (1971); 44, Stoner (1990); 45, Stoner (1992); 46, Thorson (1946); 47, Vandermeulen and DeWreede (1986); 48, Vermeij (1978); 49, Worcester (1994); 50 Zechman and Mathieson (1985).

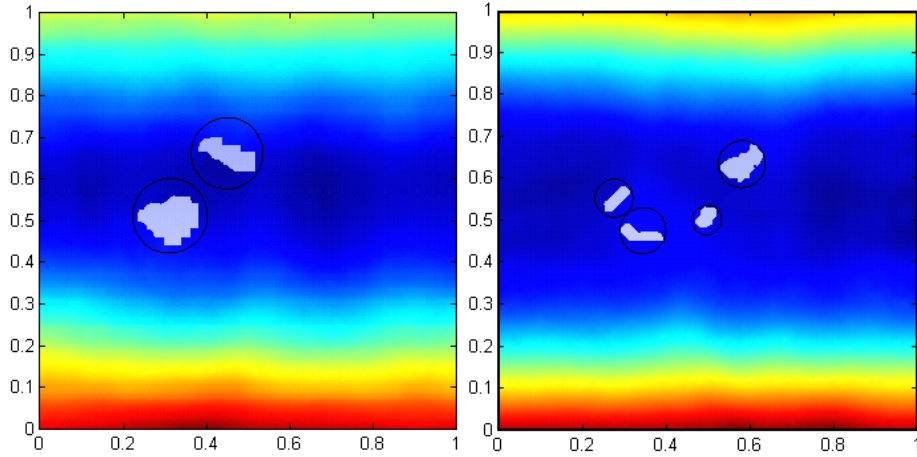


Figure 2.12: Radii around islands inside which propagules are assumed to settle

clouded by the tiny eggs and sperm. The eggs and sperm rise from the bottom of the water and form a thick layer on the surface. It is there that fertilization takes place^[20]. A longer dispersal time is therefore needed in order for the eggs to become fertilized and develop into the ‘adult phase’.

Setting different ‘passive times’ will require multiple runs, so instead, why not just check at frequent intervals (which can correspond to the ‘passive times’) where all of the particles are, build a connectivity matrix at that timestep and then allow the particles to continue to be transported by the flow? This way the evolution of the connectivity matrix can be followed, with different stages corresponding to different dispersal or passive times. This is the approach implemented by the model.

Chapter 3

Results

3.1 Two island domain

In the Stommel test case, the system became steady after about 3,000,000 time steps when energy became constant. In the case of the two and four island domains, the energy does not become constant as the elevation is being forced on the two open boundaries. A plot of the energy against the number of time steps reveals that the energy in the system oscillates:

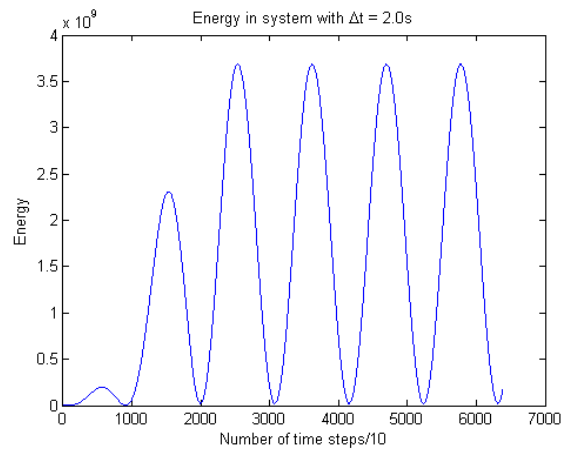


Figure 3.1: Plot of the energy in the two island system against the time step

The particles are therefore released once the energy in the simulation starts to oscillate over constant range (at 25000 time steps when Δt is set to 2.0 seconds). The results are

displayed to show the simulated dispersal times for the three types of coral larvae given in Figure (2.11) - *Pocilloporids* (4 hours), *Acroporids* (24-72 hours) and *Balanophyllia elegans* (3 days). Results are given in sets corresponding to diffusivity values 2.0, 10.0, 25.0 and 50.0 m^2s^{-1} . Plotted for each are the positions of particles and either the elevation or velocity fields for corresponding time frame. The two sets of results that best represent the behaviour for each time frame are given in this chapter, the rest can be found in Appendix A. In order to consider the islands in this domain individually, the lower island will be referred to as island one and the upper island will be referred to as island two.

3.1.1 Dispersal time = 4h (*Pocilloporids*)

Summary of results:

- for all values of the diffusivity the the particles stayed within the radii of the islands,
- as a result the connectivity matrices indicate that all propagules stayed within the vicinity of the parent reef.

Figure 3.2 displays a table of the minimum, maximum and mean distances travelled from the point of release by particles at increasing time steps.

Figure 3.2: Minimum, maximum and mean distances dispersed from initial release points for the two island domain initial four hour period

Dispersal time (mins)	Diffusivity k (m^2s^{-1})	Min. dispersal distance (m)	Max. dispersal distance (m)	Mean dispersal distance (m)
33	2.0	0.0025	0.6409	0.1336
66	2.0	0.0132	5.3517	1.0824
99	2.0	0.0239	13.7286	3.2116
132	2.0	0.0239	13.7286	3.2116
165	2.0	0.0364	24.238	6.5938
198	2.0	0.0284	22.7876	6.0714
33	10.0	0.0023	0.6076	0.1304
66	10.0	0.0095	5.3047	1.0872
99	10.0	0.0161	13.64	3.1884
132	10.0	0.0242	20.2072	5.3745
165	10.0	0.0359	23.9935	6.5632
198	10.0	0.0299	22.5723	6.053
33	25.0	0.0058	0.5531	0.1282
66	25.0	0.0103	4.9609	1.0177
99	25.0	0.0262	13.1328	3.0973
132	25.0	0.0317	19.5926	5.2509
165	25.0	0.0337	23.3111	6.4425
198	25.0	0.0266	22.817	6.2749
33	50.0	0.0084	0.6893	0.1245
66	50.0	0.0153	5.4901	1.1026
99	50.0	0.0169	14.4601	3.2979
132	50.0	0.0385	21.0021	5.5576
165	50.0	0.0494	25.0793	6.7454
198	50.0	0.0265	22.6349	6.0317

3.1.2 Dispersal time = 24h - 72h (*Acroporids*, *Balanophyllia elegans*)

Summary of results:

- At low values of diffusivity the particles still stay within the radii of the islands,
- but now at higher values of diffusivity some particles start to oscillate in and out of one of the islands.
- The two extremes are displayed, $k = 2.0\text{m}^2\text{s}^{-1}$ and $k = 50.0\text{m}^2\text{s}^{-1}$.

Minimum, maximum and mean dispersal distances are given in Figure 3.6.

3.2 Four island domain

At this point it is necessary to consider the computational and time restraints on this study. For the CFL condition to be satisfied for the four island domain, it is necessary to change the time step from $\Delta t = 2.0\text{s}$ to $\Delta t = 0.25\text{s}$, i.e. one iteration corresponds to just a quarter of a second. As a result, the time taken for the energy to oscillate between a steady range increases to 200,000 time steps (see Figure 3.5). The execution time for the program to reach this point is about 44 hours. For the program to then simulate the dispersal of particles for 72 hours would require a further 1,036,800 time steps, bringing the total execution time to about 11.5 days. This means that the time required to investigate the four island domain runs outside of the time scale of this project. Presented are the results obtained for the first four hours of dispersion time for $k = 10.0\text{m}^2\text{s}^{-1}$, along with an analysis of the connectivity matrices returned by the program at some later time steps. The islands are referred to as islands one to four, with island one being the far left island, island two the next one to the right, island three the next and island four the far right.

3.2.1 Dispersal time = 4h (*Pocilloporids*)

Summary of results:

- A similar pattern to that seen with the two island domain occurs, some particles move far enough to exit the circular zones around the islands but oscillate in and out of these zones as the dispersal time approaches four hours.
- All of the particles that ‘leave’ their islands begin at island four. These particles were released from the North-East and South-West of this island. The rest of the particles released from this island stay within the enclosing circle.

3.2.2 Longer dispersal times

The four island simulation was run until the end of the time allocated for this study, the evolution of the connectivity matrix is given below. Particles are released once the system has reached a steady state at 200,000 time steps. The final time step is 425,000 which corresponds to a simulation of propagules in the water column for 29.5 hours.

Initially, particles start to leave the fourth island and then after some time leave the third island:

$$\begin{pmatrix} 60 & 0 & 0 & 0 \\ 0 & 60 & 0 & 0 \\ 0 & 0 & 60 & 0 \\ 0 & 0 & 0 & 60 \end{pmatrix}$$

Time step = 200000

$$\begin{pmatrix} 60 & 0 & 0 & 0 \\ 0 & 60 & 0 & 0 \\ 0 & 0 & 60 & 0 \\ 0 & 0 & 0 & 41 \end{pmatrix}$$

Time step = 227000

$$\begin{pmatrix} 60 & 0 & 0 & 0 \\ 0 & 60 & 0 & 0 \\ 0 & 0 & 50 & 0 \\ 0 & 0 & 0 & 48 \end{pmatrix}$$

Time step = 250000

Particles then begin to leave the second island and others move in and out of the third and fourth islands:

$$\begin{pmatrix} 60 & 0 & 0 & 0 \\ 0 & 50 & 0 & 0 \\ 0 & 0 & 40 & 0 \\ 0 & 0 & 0 & 41 \end{pmatrix}$$

Time step = 270000

$$\begin{pmatrix} 60 & 0 & 0 & 0 \\ 0 & 50 & 0 & 0 \\ 0 & 0 & 31 & 0 \\ 0 & 0 & 0 & 40 \end{pmatrix}$$

Time step = 280000

$$\begin{pmatrix} 60 & 0 & 0 & 0 \\ 0 & 50 & 0 & 0 \\ 0 & 0 & 43 & 0 \\ 0 & 0 & 0 & 40 \end{pmatrix}$$

Time step = 300000

After 300,000 time steps particles start to return to their parent islands:

$$\begin{pmatrix} 60 & 0 & 0 & 0 \\ 0 & 50 & 0 & 0 \\ 0 & 0 & 50 & 0 \\ 0 & 0 & 0 & 47 \end{pmatrix}$$

Time step = 310000

$$\begin{pmatrix} 60 & 0 & 0 & 0 \\ 0 & 60 & 0 & 0 \\ 0 & 0 & 60 & 0 \\ 0 & 0 & 0 & 51 \end{pmatrix}$$

Time step = 330000

$$\begin{pmatrix} 60 & 0 & 0 & 0 \\ 0 & 60 & 0 & 0 \\ 0 & 0 & 60 & 0 \\ 0 & 0 & 0 & 60 \end{pmatrix}$$

Time step = 340000

Particles remain at their initial islands until 370,000 time steps when a few start to move from the first island:

$$\begin{pmatrix} 60 & 0 & 0 & 0 \\ 0 & 60 & 0 & 0 \\ 0 & 0 & 60 & 0 \\ 0 & 0 & 0 & 60 \end{pmatrix}$$

Time step = 360000

$$\begin{pmatrix} 59 & 0 & 0 & 0 \\ 0 & 60 & 0 & 0 \\ 0 & 0 & 60 & 0 \\ 0 & 0 & 0 & 60 \end{pmatrix}$$

Time step = 370000

$$\begin{pmatrix} 53 & 0 & 0 & 0 \\ 0 & 60 & 0 & 0 \\ 0 & 0 & 60 & 0 \\ 0 & 0 & 0 & 60 \end{pmatrix}$$

Time step = 380000

Particles return to their initial islands once more, and finally a few particles leave the fourth island again:

$$\begin{pmatrix} 60 & 0 & 0 & 0 \\ 0 & 60 & 0 & 0 \\ 0 & 0 & 60 & 0 \\ 0 & 0 & 0 & 60 \end{pmatrix}$$

Time step = 390000

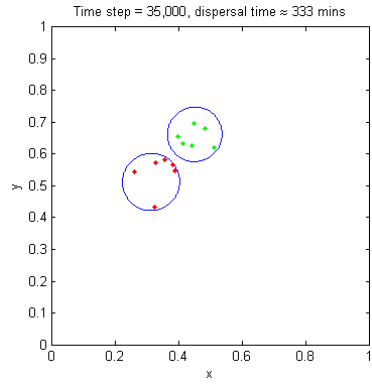
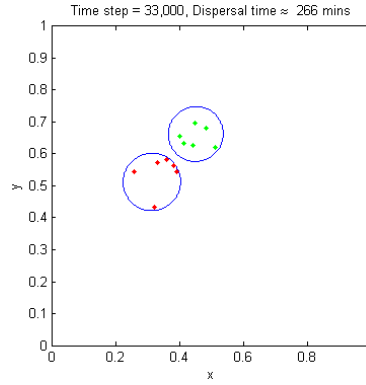
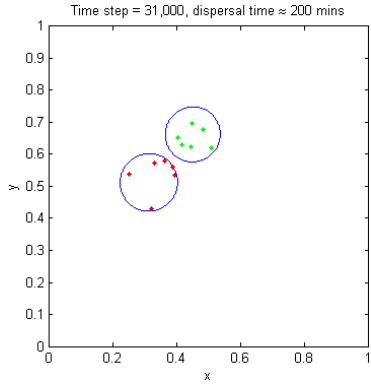
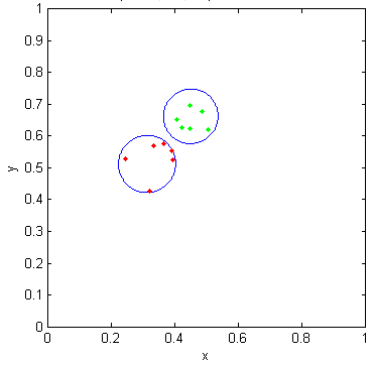
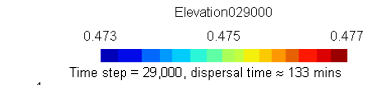
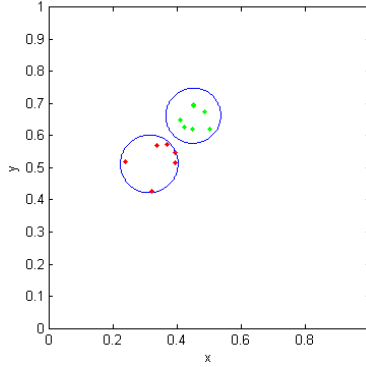
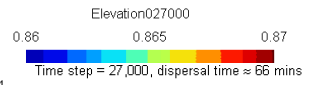
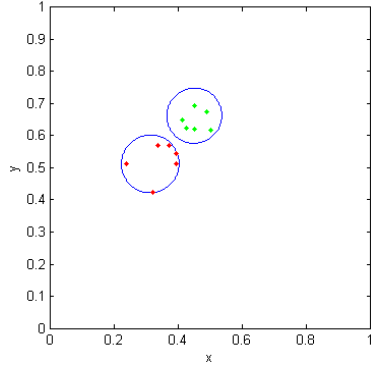
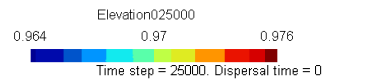
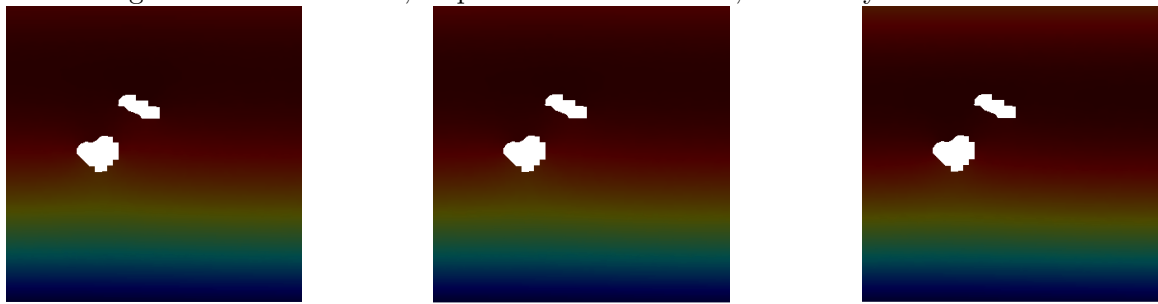
$$\begin{pmatrix} 50 & 0 & 0 & 0 \\ 0 & 60 & 0 & 0 \\ 0 & 0 & 60 & 0 \\ 0 & 0 & 0 & 50 \end{pmatrix}$$

Time step = 410000

$$\begin{pmatrix} 60 & 0 & 0 & 0 \\ 0 & 60 & 0 & 0 \\ 0 & 0 & 60 & 0 \\ 0 & 0 & 0 & 47 \end{pmatrix}$$

Time step = 425000

Figure 3.3: Two islands, dispersal time ≈ 4 hours, diffusivity $k = 2.0\text{m}^2\text{s}^{-1}$



$$\begin{pmatrix} 60 & 0 \\ 0 & 60 \end{pmatrix}$$

Time step = 25000

$$\begin{pmatrix} 60 & 0 \\ 0 & 60 \end{pmatrix}$$

Time step = 27000

$$\begin{pmatrix} 60 & 0 \\ 0 & 60 \end{pmatrix}$$

Time step = 29000

$$\begin{pmatrix} 60 & 0 \\ 0 & 60 \end{pmatrix}$$

Time step = 31000

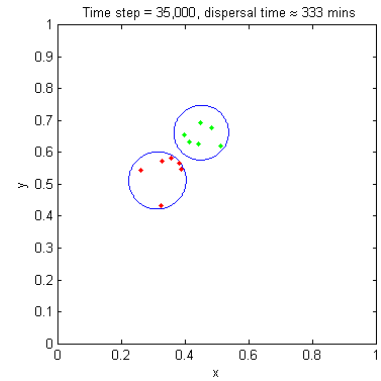
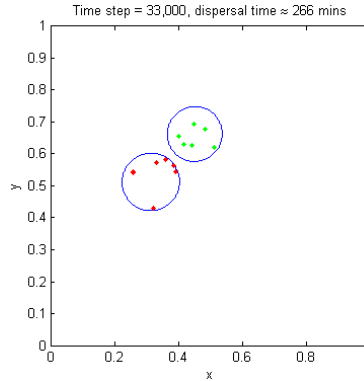
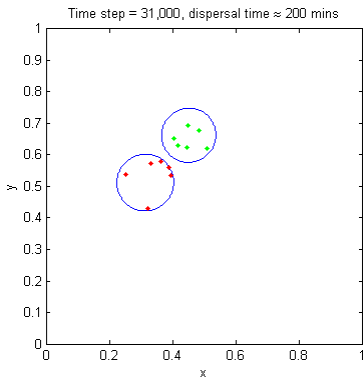
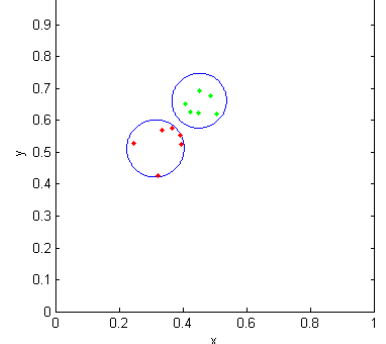
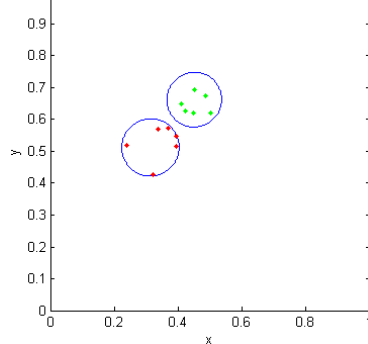
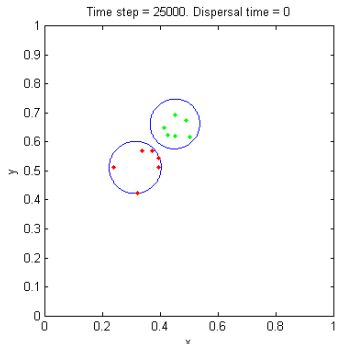
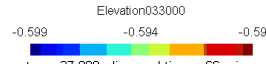
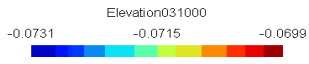
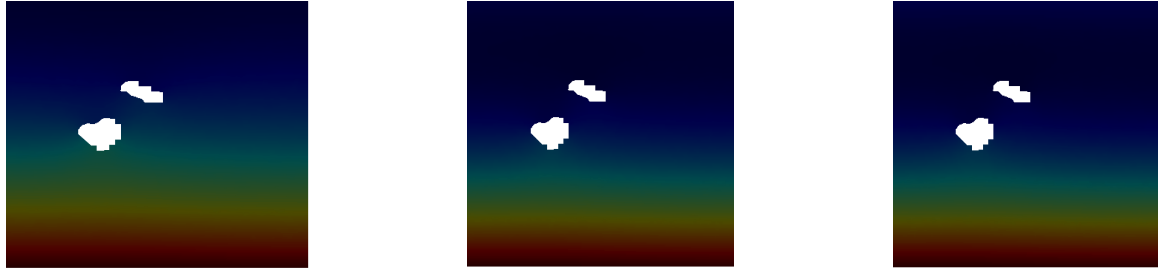
$$\begin{pmatrix} 60 & 0 \\ 0 & 60 \end{pmatrix}$$

Time step = 33000

$$\begin{pmatrix} 60 & 0 \\ 0 & 60 \end{pmatrix}$$

Time step = 35000

Figure 3.4: Two islands, dispersal time $\approx 4\text{h}$, diffusivity $k = 10.0\text{m}^2\text{s}^{-1}$



$$\begin{pmatrix} 60 & 0 \\ 0 & 60 \end{pmatrix}$$

Time step = 25000

$$\begin{pmatrix} 60 & 0 \\ 0 & 60 \end{pmatrix}$$

Time step = 27000

$$\begin{pmatrix} 60 & 0 \\ 0 & 60 \end{pmatrix}$$

Time step = 29000

$$\begin{pmatrix} 60 & 0 \\ 0 & 60 \end{pmatrix}$$

Time step = 31000

$$\begin{pmatrix} 60 & 0 \\ 0 & 60 \end{pmatrix}$$

Time step = 33000

$$\begin{pmatrix} 60 & 0 \\ 0 & 60 \end{pmatrix}$$

Time step = 35000

Figure 3.5: Minimum, maximum and mean distances dispersed from initial release points for the two island 24-72 hour period

Dispersal time (hours)	Diffusivity k (m^2s^{-1})	Min. dispersal distance (m)	Max. dispersal distance (m)	Mean dispersal distance (m)
24	2.0	0.0058	2.195	0.2774
32	2.0	0.0332	15.6949	3.9506
40	2.0	0.0462	14.2177	3.7792
48	2.0	0.0039	4.8538	0.547
56	2.0	0.0289	9.9643	2.6251
64	2.0	0.0513	9.8873	3.0289
72	2.0	0.0135	11.5694	1.3148
24	10.0	0.0381	2.061	0.3169
32	10.0	0.0842	15.6139	3.8381
40	10.0	0.1153	14.0795	3.7566
48	10.0	0.0663	3.3277	0.5675
56	10.0	0.1481	9.3197	2.7039
64	10.0	0.1911	8.4765	3.0071
72	10.0	0.1633	14.1498	1.9294
24	25.0	0.1631	5.9783	1.0512
32	25.0	0.43	13.7862	4.4041
40	25.0	0.3488	12.1079	4.415
48	25.0	0.2084	9.9376	1.8077
56	25.0	0.5233	7.858	3.2991
64	25.0	0.5443	37.5167	6.728
72	25.0	0.2543	22.9991	3.6855
24	50.0	0.0168	27.8431	4.0759
32	50.0	0.0868	13.2853	3.7334
40	50.0	0.1322	11.6651	3.7061
48	50.0	0.109	48.843	4.0699
56	50.0	0.077	6.3922	2.7601
64	50.0	0.3656	78.3352	8.6435
72	50.0	0.5258	20.2717	4.6574

Figure 3.6: Two islands, dispersal time $\approx 24\text{-}72\text{h}$, diffusivity $k = 2.0\text{m}^2\text{s}^{-1}$

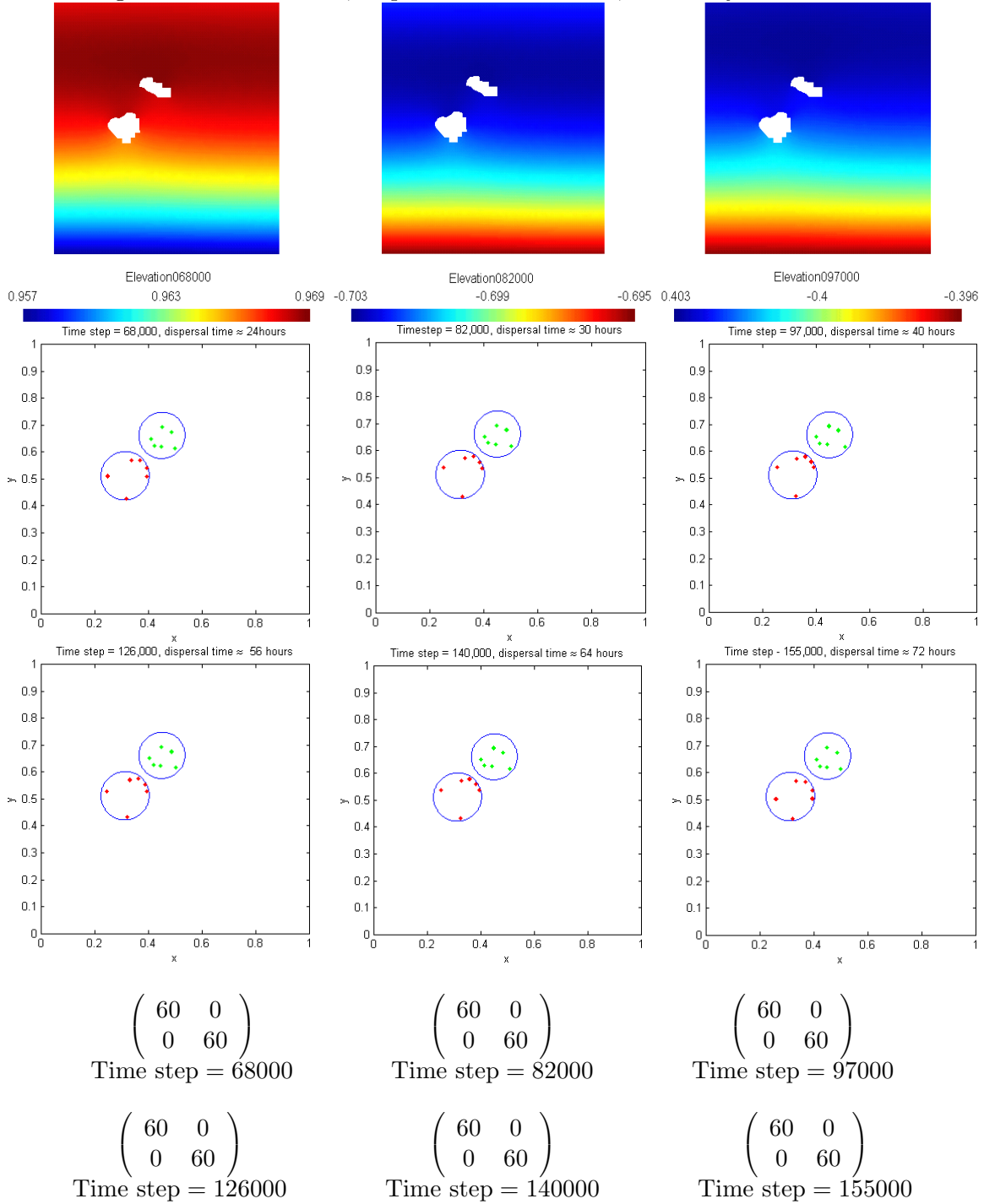
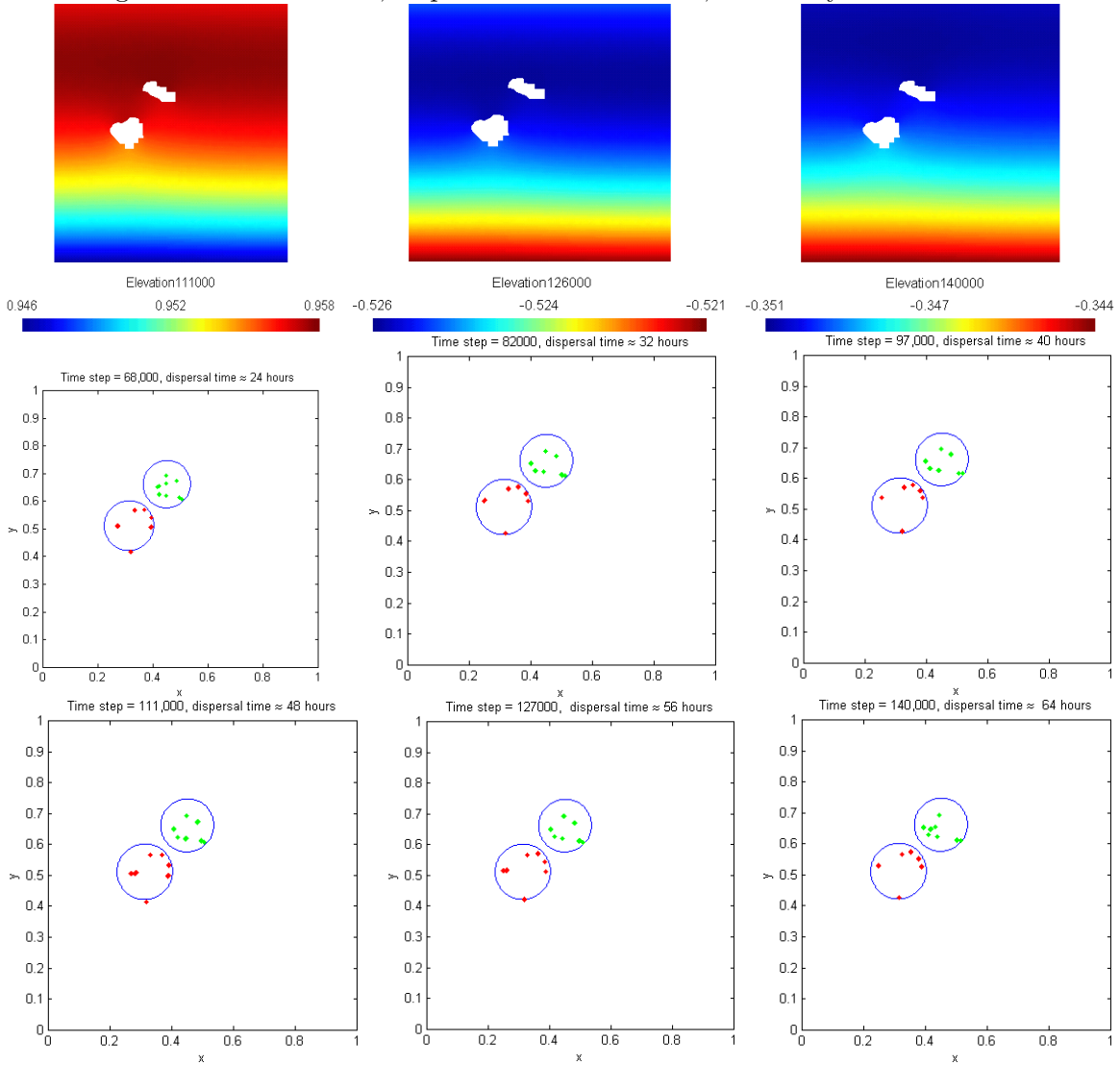


Figure 3.7: Two islands, dispersal time $\approx 24\text{h}-72\text{h}$, diffusivity $k = 50.0\text{m}^2\text{s}^{-1}$



$$\begin{pmatrix} 50 & 0 \\ 0 & 60 \end{pmatrix}$$

Time step = 68000

$$\begin{pmatrix} 60 & 0 \\ 0 & 60 \end{pmatrix}$$

Time step = 82000

$$\begin{pmatrix} 60 & 0 \\ 0 & 60 \end{pmatrix}$$

Time step = 97000

$$\begin{pmatrix} 50 & 0 \\ 0 & 60 \end{pmatrix}$$

Time step = 111000

$$\begin{pmatrix} 54 & 0 \\ 0 & 60 \end{pmatrix}$$

Time step = 127000

$$\begin{pmatrix} 60 & 0 \\ 0 & 60 \end{pmatrix}$$

Time step = 140000

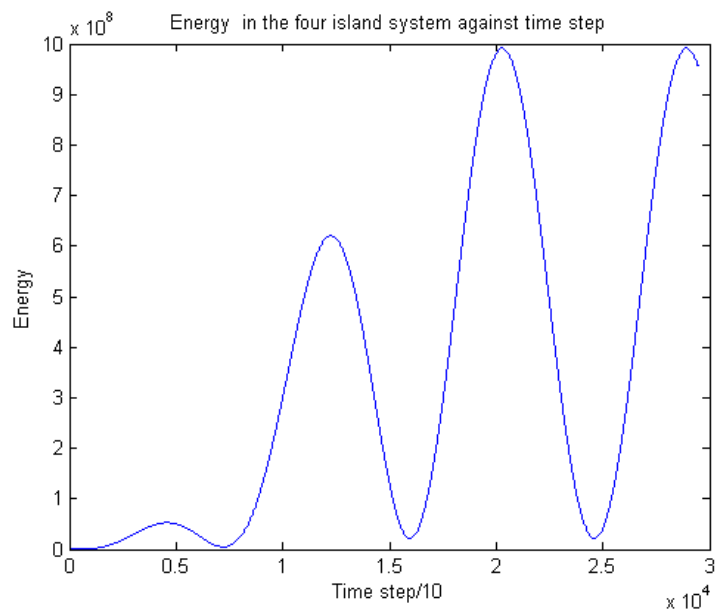
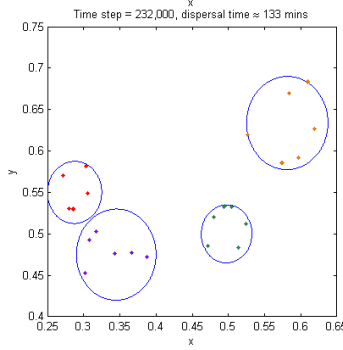
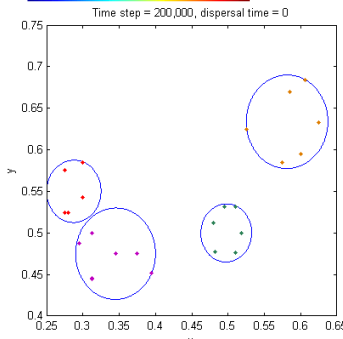
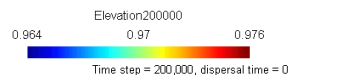
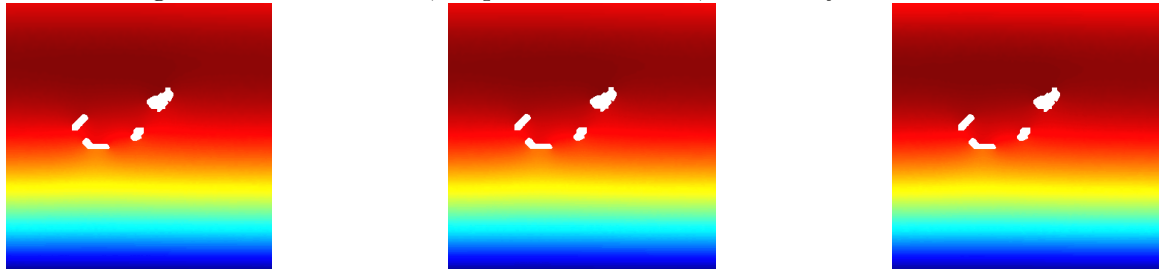


Figure 3.8: Energy in the four island system

Figure 3.9: Four islands, dispersal time $\approx 4\text{h}$, diffusivity $k = 10.0\text{m}^2\text{s}^{-1}$

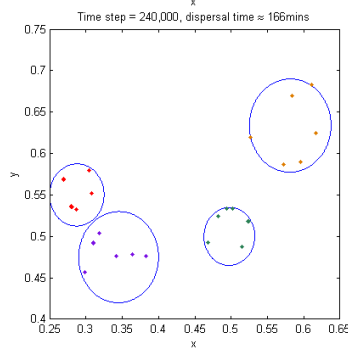
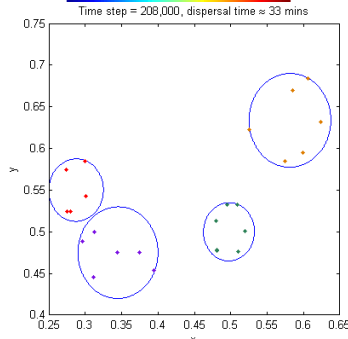
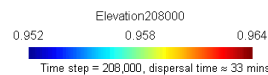
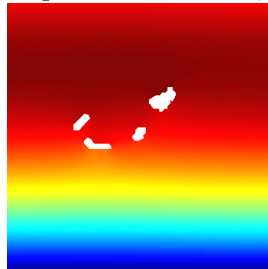


$$\begin{pmatrix} 60 & 0 & 0 & 0 \\ 0 & 60 & 0 & 0 \\ 0 & 0 & 60 & 0 \\ 0 & 0 & 0 & 60 \end{pmatrix}$$

Time step = 200000

$$\begin{pmatrix} 60 & 0 & 0 & 0 \\ 0 & 60 & 0 & 0 \\ 0 & 0 & 60 & 0 \\ 0 & 0 & 0 & 50 \end{pmatrix}$$

Time step = 232000

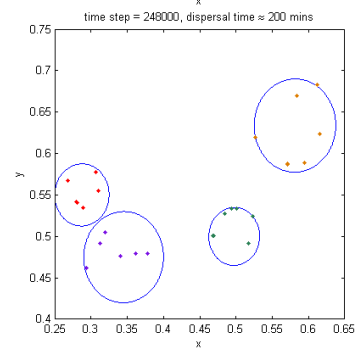
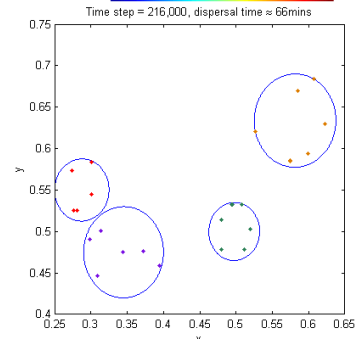
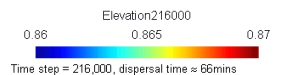
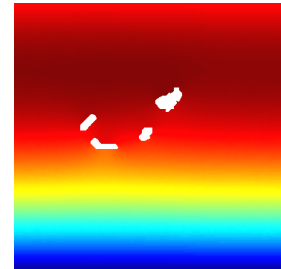


$$\begin{pmatrix} 60 & 0 & 0 & 0 \\ 0 & 60 & 0 & 0 \\ 0 & 0 & 60 & 0 \\ 0 & 0 & 0 & 50 \end{pmatrix}$$

Time step = 208000

$$\begin{pmatrix} 60 & 0 & 0 & 0 \\ 0 & 60 & 0 & 0 \\ 0 & 0 & 60 & 0 \\ 0 & 0 & 0 & 42 \end{pmatrix}$$

Time step = 240000



$$\begin{pmatrix} 60 & 0 & 0 & 0 \\ 0 & 60 & 0 & 0 \\ 0 & 0 & 60 & 0 \\ 0 & 0 & 0 & 48 \end{pmatrix}$$

Time step = 216000

$$\begin{pmatrix} 60 & 0 & 0 & 0 \\ 0 & 60 & 0 & 0 \\ 0 & 0 & 60 & 0 \\ 0 & 0 & 0 & 48 \end{pmatrix}$$

Time step = 248000

Chapter 4

Discussion of results and conclusions

4.1 The two island domain

4.1.1 The four hour simulation

In general, particles did not leave the vicinity of their initial islands during the four hour simulation. This was not surprising, as, according to Figure 2.11, the coral species that has a dispersal time of four hours, *Pocilloporids*, has a mean dispersal distance $\leq 0.6\text{km}$. The simulated dispersal distances turned out to be much smaller than this - none of the particles dispersed further than 25m away from the point of release. The reason for this seems to be that the particles started to move away from the point of release but were then carried back by the flow. This can be seen in Figure 3.2 where the maximum and average dispersal distances increase steadily up to 165 minutes, but decrease at 198 minutes for each value of the diffusivity.

The connectivity matrices seem to imply that every particle settled on the parent island, i.e. if the model was accurately simulating the dispersal of *Pocilloporids* larvae and if the islands were made up entirely of *Pocilloporids* corals, then they would be self seeding. However, it is important to remember that these connectivity matrices only show that the particles are within certain radii of the islands. So although the information on the dispersal of *Pocilloporids* larvae suggests that the larvae should settle on or near the parent islands, and that

the model is simulating this, it must be noted that the method of using radii inside which particles are assumed to settle is purely hypothetical, and so this is of course speculation.

4.1.2 The 24-72 hour simulation

In the 24-72 hour simulation, corresponding to the dispersal times for *Acroporids* (24-72 hours) and *Balanophyllia elegans* (72 hours), whether or not particles left the vicinity of the islands depended on value of the diffusivity k . At a value of $k = 50\text{m}^2\text{s}^{-1}$ particles started to leave the lower island. However, having left the vicinity of the island they then proceeded to return, leave again and then slowly return by the end of the 72 hour time frame. This oscillating behaviour can also be seen for all of the other values of k in the table given in Figure 3.6. For dispersal times up to 40 hours, the maximum and average dispersal distances increase but then drop at 48 hours. For the remaining 24 hours the maximum and average dispersal distances rise and fall as the particles move back and forth.

So do the model simulations represent the behaviour of either *Balanophyllia elegans* larvae or *Acroporids* larvae? The distances travelled by the particles indicate that the simulations are closer to that of the *Acroporids* larvae. Of course the dispersal distances for this larvae are only really relevant to the regions where the data was sourced from (Rib Reef, Pandora Reef and Myrmidon Reef in the Great Barrier Reef, Australia, Sammarco and Andrews (1989)), not necessarily the simple two island domain in this study! A further study could simulate the dispersal of particles in the aforementioned reefs in the GBR in order to either confirm this observation or tailor the model to accurately simulate the dispersal of *Acroporids* larvae.

As far as simulating the dispersal of *Balanophyllia elegans* larvae is concerned, a more complex algorithm would be required to simulate larvae moving just 0.1-0.5m in 72 hours. Construction of such an algorithm would require research into how these corals reproduce and what keeps the larvae so close to the reefs for three days.

4.2 The four island domain

4.2.1 The four hour simulation

Results obtained for this simulation were similar to the four hour simulation in the two island domain - the majority of the particles stayed within the zones drawn around the islands. A few particles did leave the fourth island - between 33 minutes and 200 minutes particles on the North-East and South-West of island four moved in and out of the perimeter.

4.2.2 Longer simulations

In the 30 hours that the particles in the four island domain were in the water column, the general behaviour exhibited reflects that observed in all of the simulations so far - the particles do not move far from the vicinity of the islands of their release - when they do they tend to oscillate in and out of the circles enclosing the islands. This oscillatory motion is probably due to the flow taking the particles out of the island zones when the elevation is forced on one open boundary, and then pushing them back in when the elevation is forced on the opposite open boundary when the ‘tide’ is reversed.

The island that experienced the most activity in this domain was island four. This could have been because:

- this island is the closest to an open boundary and so experiences the greatest velocities,
or
- the perimeter drawn around this island was closer to the release points than in the other domains and so the particles did not have to travel as far to leave the vicinity of the island, or
- this island is the furthest from any other island and so small scale features such as eddies in the wake of other islands do not interfere significantly with the flow around this island.

4.3 Summary of conclusions

Factors that could be taken into account when building a connectivity matrix for the Great Barrier Reef could be:

- The type of coral larvae being dispersed. The species of corals with the highest population in each island or reef could be simulated.
- The different dispersal strategies - both the long range and short range strategies could be taken into account, this would require a model that simulates a the dispersal of coral larvae over a long period of time ($> 300h$ or even as far as a yearly dispersal distance) while keeping track of species of larvae that only disperse short distances.

Chapter 5

Further work

In addition to the suggestions made in Chapter 4, further work that could be done directly on this project is summarised in the sections that follow.

5.1 The modified Lagrangian algorithm

In this study the Lagrangian algorithm was used to update the position of particles:

$$\mathbf{x}_{n+1} = \mathbf{x}_n + \mathbf{v}\Delta t + \frac{\mathbf{R}_n}{\sqrt{r}}\sqrt{2k\Delta t} \quad (5.1)$$

This algorithm assumes a constant diffusivity k and depth h . This is not ideal for the domains studied as the depth changes with the elevation and the bathymetry of the islands, and the diffusivity will vary according to how far the particles are from the islands (i.e. how far they are from the turbulent features such as eddies in the wake of islands). An algorithm could be implemented to include varying h and k . It is noted in [6] that when h or k is not constant the Lagrangian algorithm (5.1) tends to accumulate particles in regions where h or k is small. To correct this a modified Lagrangian algorithm should be used.

The modified Lagrangian algorithm makes corrections to (5.1) so that the concentration of particles tends toward the concentration derived from the Eulerian equation. To obtain the modified Lagrangian algorithm, rewrite the Eulerian equation

$$\frac{\partial(hc)}{\partial t} = -\nabla \cdot (\mathbf{u}hc - hk\nabla c) \quad (5.2)$$

as

$$\frac{\partial(hc)}{\partial t} = -\nabla \cdot [(\mathbf{u} + kh^{-1}\nabla h)hc - k\nabla(hc)]. \quad (5.3)$$

Equation (5.3) can be considered as an advection-diffusion equation for which the quantity to be transported is hc , and the advection velocity is $\mathbf{u} + kh^{-1}\nabla h$ (Spagnol et al., 2002). If the depth h varies in space, the equivalent particle tracking algorithm then takes the same form as equation (5.1), with the velocity \mathbf{v} taken as

$$\mathbf{v} = \mathbf{u} + \frac{h}{k}\nabla h, \quad (5.4)$$

(Spagnol et al., 2002) where \mathbf{u} is the depth averaged horizontal water velocity (returned by the model). If the diffusivity also varies in space then the velocity \mathbf{v} takes the form:

$$\mathbf{v} = \mathbf{u} + \frac{h}{k}\nabla h + \nabla k, \quad (5.5)$$

(Spagnol et al., 2002).

5.2 Areas representing the islands

The radii drawn around each island are a very simple way of representing the islands in this study. These circles enclose some islands more tightly than others, resulting in the distance a particle needs to be from an island to attach varying. More complicated shapes that closely follow the shorelines could be used in order to get a more accurate estimate of when the particles reach the island.

5.3 A mortality rate

Not all of the coral larvae survive to attach to a reef as they are prey to other marine life. A mortality rate to simulate this could be implemented by assigning to each propagule a probability p that it will live (where p is between zero and one) and producing a random number q between zero and one every n time steps. If $q > p$ then the propagule lives and carries on until the next n time steps are complete when another random number is generated to decide its fate. If $q < p$ then the propagule dies and is omitted from the simulation for the remaining time steps.

5.4 Different species of Coral

The coral species mentioned in this study all have small dispersal distances and times relative to the distances and times that would be considered when thinking about designing marine reserves. Shanks et al. (2003) mentions two evolutionary stable dispersal strategies: dispersal $< 1\text{km}$ with propagules spending less than 100 hours in the water column, or $> 20\text{km}$ with propagules spending over 300 hours in the water column. Much longer simulations could be run in order to investigate corals whose larvae travel distances over 20km.

Appendix A

Included in this appendix are the remaining plots of particle positions for the two island four hour and 72 hour simulations.

Figure 5.1: Two islands, dispersal time $\approx 4\text{h}$, diffusivity $k = 25.0\text{m}^2\text{s}^{-1}$

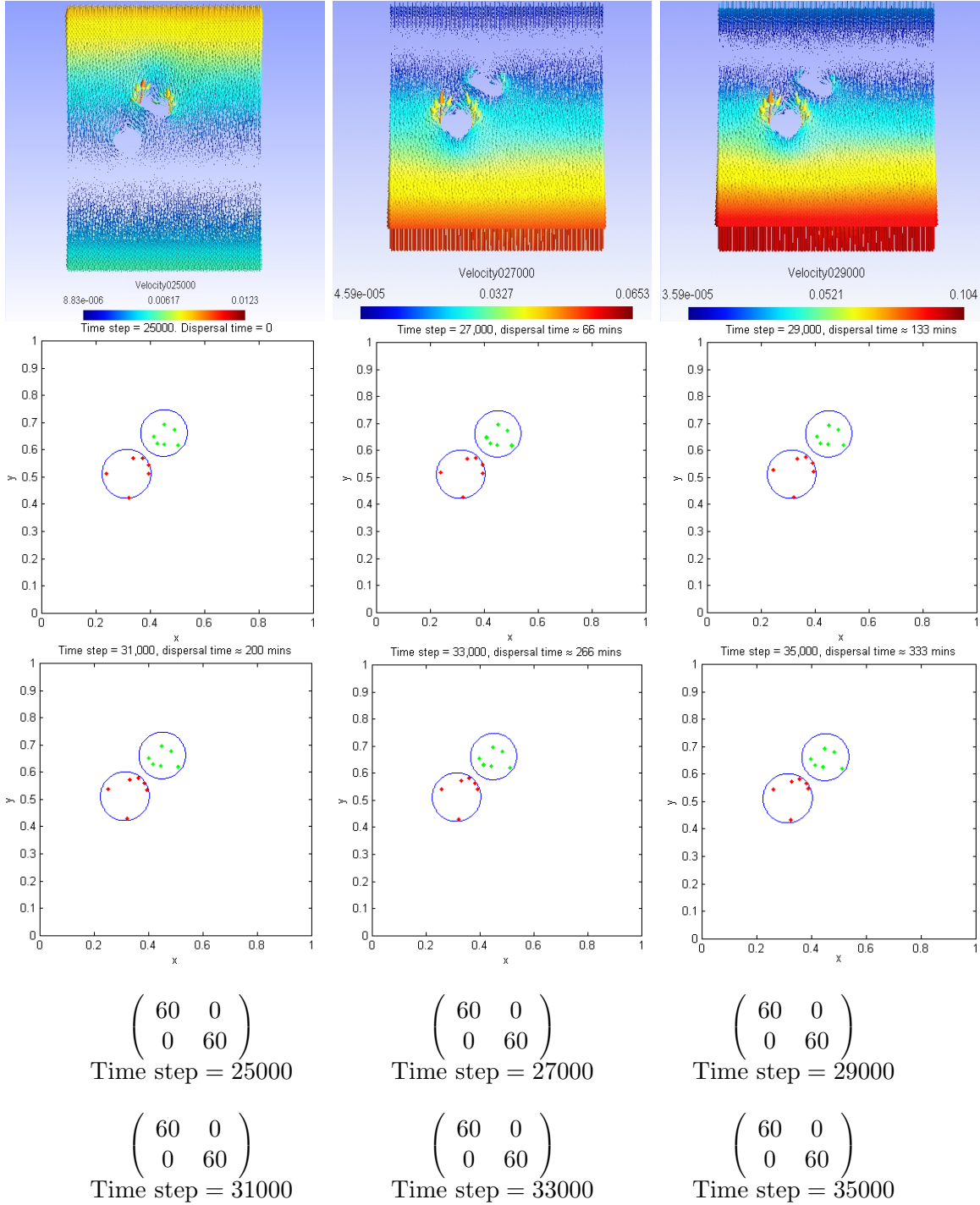


Figure 5.2: Two islands, dispersal time $\approx 4\text{h}$, diffusivity $k = 50.0\text{m}^2\text{s}^{-1}$

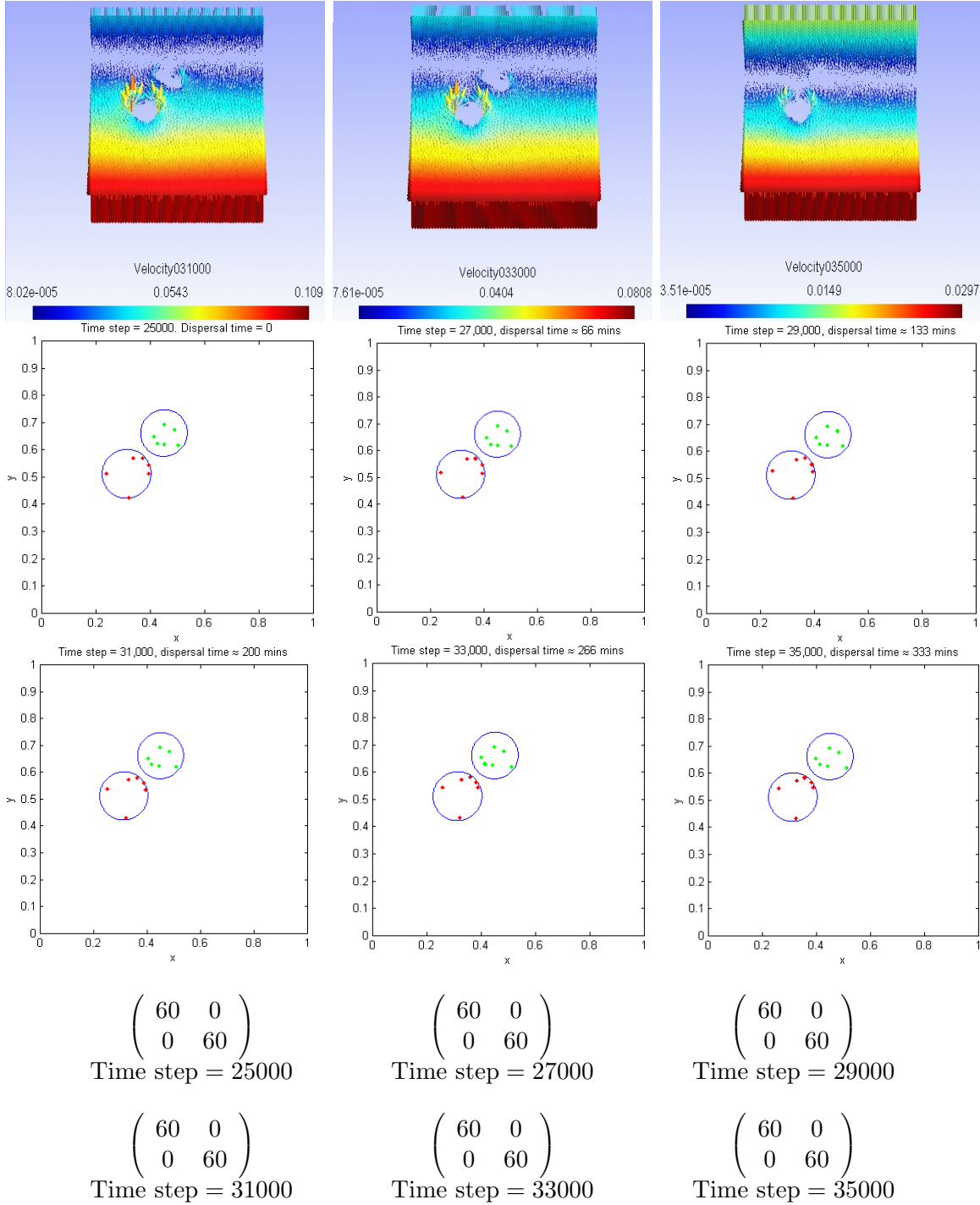


Figure 5.3: Two islands, dispersal time ≈ 24 -72h, diffusivity $k = 10.0\text{m}^2\text{s}^{-1}$

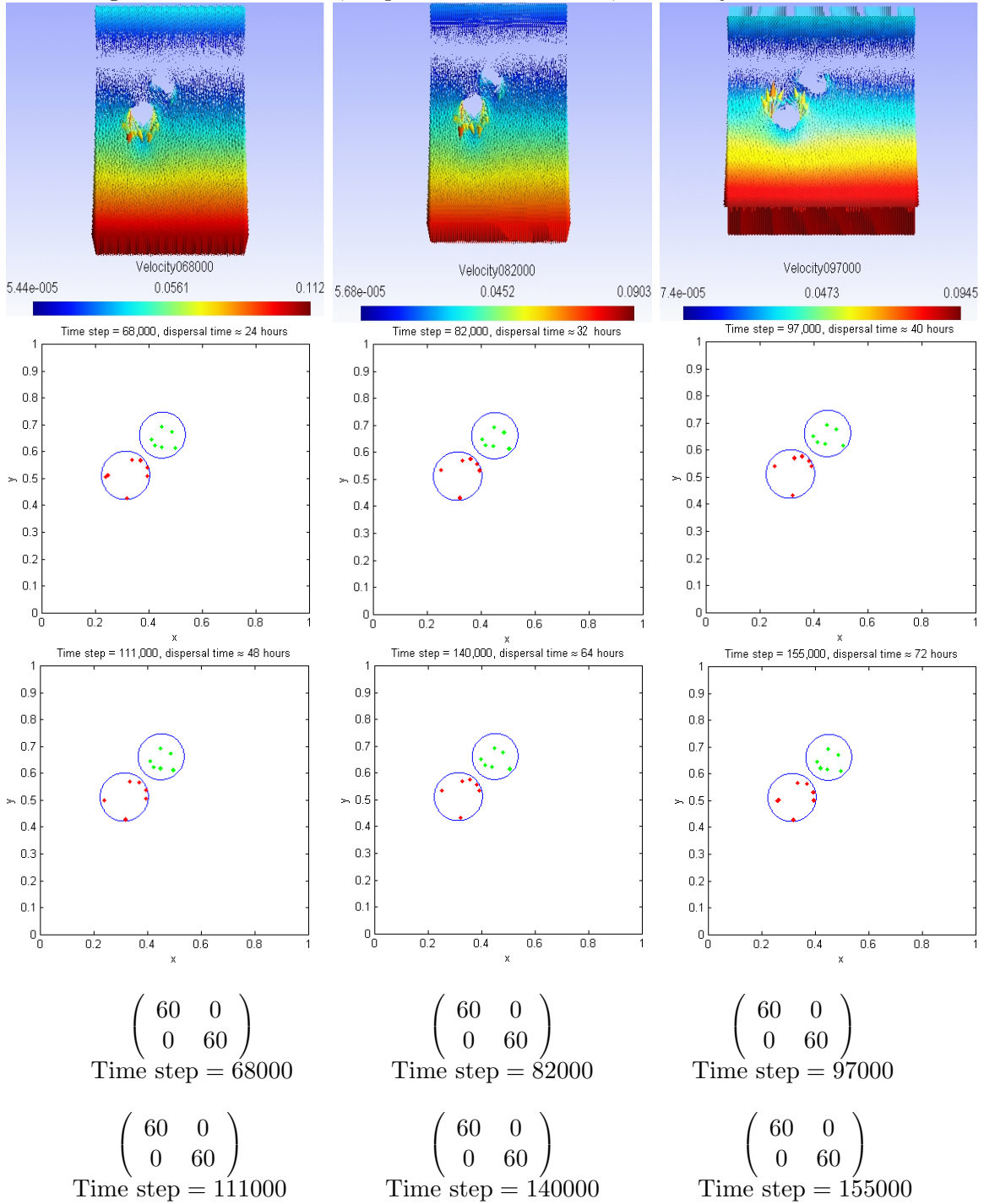
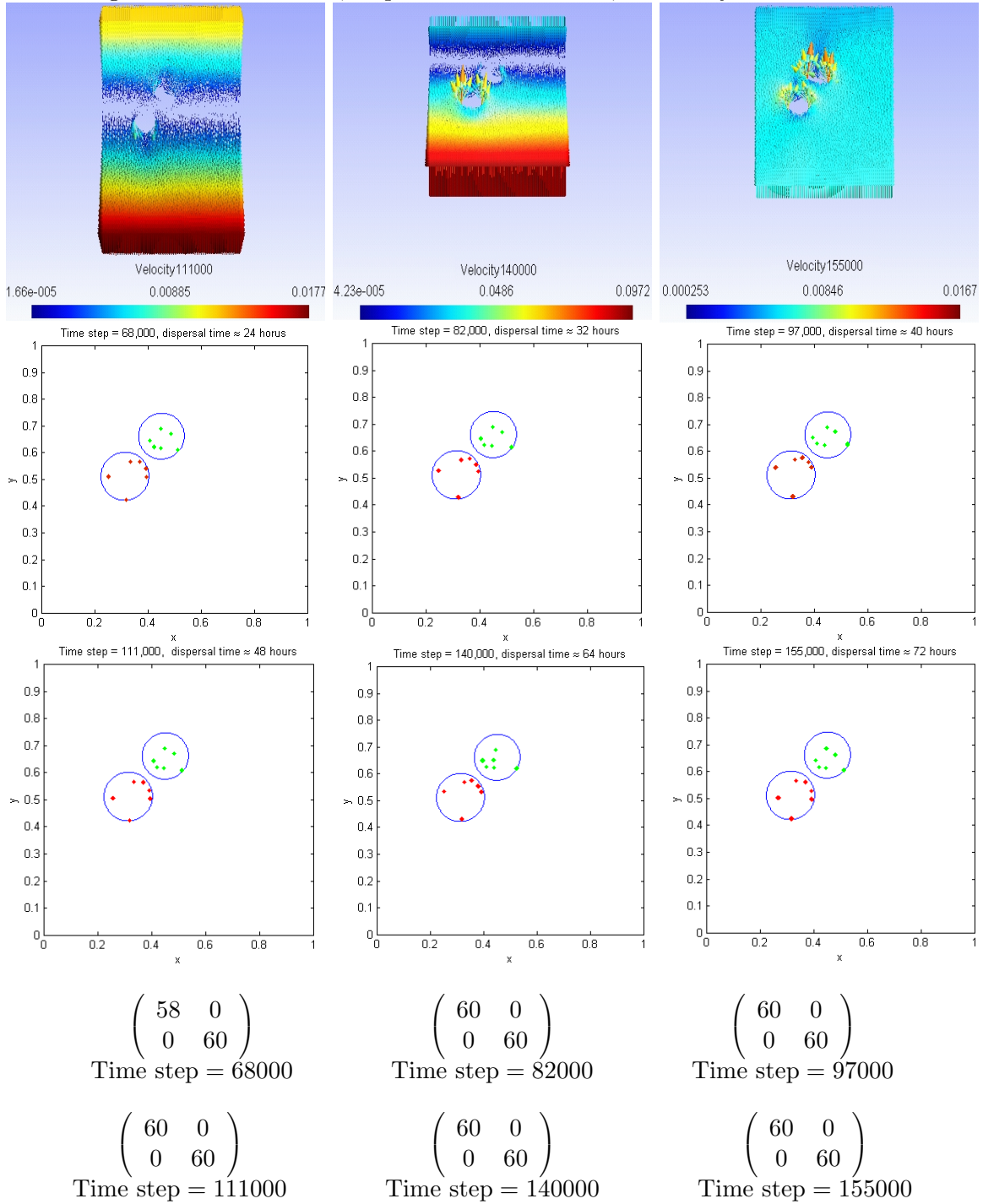


Figure 5.4: Two islands, dispersal time ≈ 24 -72h, diffusivity $k = 25.0\text{m}^2\text{s}^{-1}$



Bibliography

- [1] LAMBRECHTS, J., HANERT, E., DELEERSNIJDER, E., BERNARD, P., LEGAT, V., REMACLE, J., AND WOLANSKI, E., 2008. A multi-scale model model of the hydrodynamics of the whole Great Barrier Reef. *Estuarine, Coastal and Shelf Science*, 79, 143-151.
- [2] WOLANSKI, E., 1994 Physical Oceanographic Processes of the Great barrier Reef. *CRC Press, Boca Raton, Florida, 194pp*
- [3] HANERT, E., LE ROUX, D., LEGAT, V., DELEERSNIJDER, E., 2005. An efficient finite element method for the shallow water equations. *Elsevier, Ocean Modelling* 10, 115-136
- [4] HANERT, E., LEROUX, D.Y., LEGAT, V., DELEERSNIJDER, E., 2004. Advection schemes for unstructured grid ocean modelling. *Ocean Modelling* 7, 39-58.
- [5] HOUSTON, P., SCHWAB, C., SULI, E., 2000. Discontinuous *hp*-finite element methods for advection diffusion problems. *Tech. Rep. NA-00/15, Oxford University*.
- [6] SPAGNOL, S., WOLANSKI, E., DELEERSNIJDER, E., BRINKMAN, R., MCALLISTER, F., CUSHMAN-ROISIN, B., HANERT, E., 2002 An error frequently made in the evaluation of advective transport in two-dimensional Lagrangian models of advection-diffusion in coral reef waters. *Marine Ecology Progress Series, Vol 235: 299-302*
- [7] SAMMARCO, P.W., ANDREWS J.C., 1988. Localised dispersal recruitment in Great Barrier Reef corals: the Helix experiment. *Science* 239:1422-1424
- [8] SAMMARCO, P.W., ANDREWS J.C., 1989. The Helix experiment: differential localized dispersal and recruitment patterns in Great Barrier Reef corals . *Limnology and Oceanography* 34:896-912

- [9] WOLANSKI, E., BURRAGE, D., KING, B., 1989 Trapping and dispersal of coral eggs around Bowden Reef, Great Barrier Reef, following mass spawning. *Cont Shelf Res* 9:479-496
- [10] WOLANSKI, E., DOHERTY, P., CARLETON, J., 1997 Directional swimming of fish larvae determines connectivity of fish populations on the Great Barrier Reef. *Naturwissenschaften* 84:262-282
- [11] The 'Point in triangle test'. <http://www.blackpawm.com/texts/pointinpoly/default.html>
- [12] BLACK, K.P., GAY, S.G., ANDREWS J.C., 1990 Residence times of neutrally buoyant matter such as larvae, sewage or nutrients on coral reefs. *Coral Reefs* 9:105-114
- [13] BLACK K.P., MORGAN P.J., HAMMOND, L.S., 1991 Numerical models show coral reefs can be self-seeding. *Mar Ecol Prog Ser* 74:1-11
- [14] BLACK K.P, 1993 The relative importance of local retention and inter-reef dispersal of neutrally buoyant material on coral reefs. *Coral reefs* 12:43-53
- [15] DIGHT I.J., JAMES M.K., BODE, L., 1990. Modelling the larval dispersal of *Acanthaster planci*. II. Patterns of reef connectivity *Coral Reefs* 39:125-134
- [16] OLIVER J., KING, B., WILLIS, B., BABCOCK, R., WOLANSKI, E., 1992. Dispersal of coral larvae from a coral reef: comparison between model predictions and observed concentrations. *Cont Shelf Res* 12:873-891
- [17] SHANKS A.L., GRANTHAM A.B., CARR, M.H, 2003 Propagule dispersal distance and the size and spacing of marine reserves. *Ecological Applications*, 13(1) 159-169
- [18] BRYANT, D., BURKE, L., MCMANUS J., SPALDING, M., 1998. Reefs at Risk: A map-based indicator of threats to the world's coral reefs. *Washington DC: World Resources Institute*
- [19] [HTTP://WWW.ZZFORKIDS.COM/ANIMALS/B/BALANOPHYLLIA_ELEGANS/](http://www.zzforkids.com/animals/B/BALANOPHYLLIA_ELEGANS/) Balanophyllia Elegans *Last Revised: 2008-07-22*
- [20] [HTTP://SANPEDROSUN.NET/OLD/98-331.HTML](http://SANPEDROSUN.NET/OLD/98-331.HTML) Orgy on the Reef - Sex Crazy Belizean Coral